Diplomarbeit

An advective-diffusive PDE Model of Starfish Feeding Fronts invading Mussel Beds in the Limfjord - Numerical Simulations & Analytical Results

ausgeführt am Institut für Analysis und Scientific Computing
der Technischen Universität Wien

unter der Anleitung von
Ao.Univ.Prof. Dipl.-Ing. Dr. Felix Breitenecker

durch
Mag. Bettina Wimmer
Kohlbachweg 3
4600 Thalheim

Wien, 5. Dezember 2014

Nous naissons tous fous,
quelques-uns le demeurent.

En attendant Godot
(Samuel Beckett, 1906-1989)

Nat og dag, vinter og sommer er den over mig -
denne dragende hjemvé efter havet.

Fruen fra Havet
(Henrik Ibsen, 1828-1906)

Preface

On 29^{th} September 2004, I decided to study Technische Mathematik at Vienna University of Technology. My first exam was on population dynamics in whale populations.

In February 2010, I applied for an IAESTE internship at DTU Aqua (Denmarks Tekniske Universitet). I did not get it, because I was only on second position in the candidate ranking. My interest was sparked. My motivation to somehow make it there anyway as well.

It was a long journey on somehow intricate paths which eventually resulted in me writing this master thesis at DTU in 2014 and at the same time concluding the Diplomstudium I started 10 years ago in Vienna. It was a journey with some detours and sidesteps. A journey leading en passant to a master degree in musicology, hundreds of concert visits in all sorts of genres, a collaboration in an article on leishmaniasis infection dynamics carried out in Spain, university lectures in five different countries, classes in linguistics, working as a teaching assistant, seminars on the translation of Danish poetry, a growing admiration for the elegance of the French language and its literature, choir singing, an enduring fascination for the sea & the Danish vadehav in particular and last but not least lots of volleyball.

I am extremely glad and thankful that by writing this master thesis in Denmark, it was possible to twist, entangle and combine my various interests and somehow make all those pieces fall into place: the sea, the languages, the marine animals, the math & the rest.

The project on which this master thesis is based was carried out under the supervision of Uffe Høgsbro Thygesen during a 10-month stay at DTU covered by the Cultural Agreements Programme. I would like to thank him for the idea to this project, his motivation and his willingness to advise me in this cross-border master thesis. I would also like to thank my Austrian supervisor Felix Breitenecker for embracing this unusual master thesis project and his involvement in it.
Further, I would like to thank Paula Canal Vergés and Finn Bak (both DSC Nykøbing Mors) as well as Bjarne Stage and Jacopo Bridda (both DTU Aqua) for giving me the possibility to take part in a mussel counting excursion at the Limfjord, where I could experience data acquisition and biological field work ”i bølgehøjde”.

It goes without saying that during those 10 years numerous people accompanied, supported and encouraged me. And not less important cheered me up, diverted me, made me laugh and smile. I am thankful to every one of them.

But in particular, I want to thank the handful of people who were at my side from the beginning to the end of this time span. And all those, who made my time in Denmark so joyful, inspiring and worthwhile.

Tusind tak.
Merci bien.
Herzlichen Dank.
Thank you very much.
This master thesis is dedicated to you.

Bettina Wimmer
DTU Library in Kongens Lyngby
25^{th} June 2014

revised in Oslo
2^{nd} November 2014

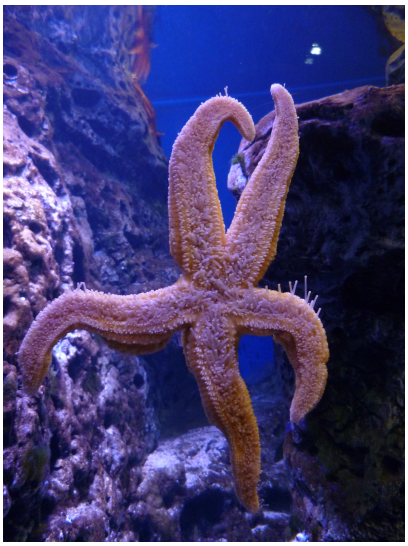

Starfish at Den Blå Planet, Amager
(Denmark's National Aquarium)

En attendant god ost.

Contents

1 Introduction

The aim of this master thesis is to describe patterns occurring in starfish populations invading mussel beds in the Limfjord. It has been observed that starfish form wavelike patterns, called *feeding fronts*, a phenomenon also known by other seawater creatures such as urchins, see Abraham (2007) or Scheibling and Lauzon-Guay (2007). Figure (1) shows such a starfish accumulation. There are various articles dealing with biological facts about those starfish wavefront observations (e.g. Dare (1982)). However, only few models aim to describe this phenomenon in particular.

Figure 1: Starfish feeding front as described by Lauzon-Guay et al. (2008), photo credit: R. Scheibling

The Danish Limfjord in Northern Jylland is famous for its mussels and oysters. Hence, starfish feeding on mussels threaten the harvest of the latter. Therefore it is of great interest to the government as well as fishers and the mussel industry to know about the starfish moving patterns. This thesis will present a partial differential equation model, which is based on starfish diffusion and mussel harvesting. The idea was to keep biological assumptions on the ecosystem as low as possible. It turns out that these very elementary

dynamics are already sufficient to evoke wavelike behaviour in the starfish population, when they exploit mussel beds. However, these waves are not traveling waves in the classical sense of partial differential equations (PDE) theory. To obtain traveling waves in the common definition it is necessary to make very specific biological assumptions, which cannot be taken for granted in real life.

The thesis starts with an overview on the biological premises and basic information on mussels, starfish and the Danish Limfjord (chapter (2)), followed by a short introduction on wave phenomena in an advection-diffusion context (chapter (3)). In chapter (4), the advective-diffusive PDE model to describe the starfish invading the mussel beds will be introduced. A core part of this thesis are the subsequent simulations, which are presented in chapter (5). Their solutions will be analyzed in detail in chapter (6). An important analytical result is the absence of traveling waves in this model as shown in chapter (7). Further, the influence of the diffusivity function on the system's stability in a scenario with mussel growth will be investigated in chapter (8). Of high interest is the comparison to other scientists' results in chapter (9). It will be explained how they actually achieved to obtain traveling wave solutions in comparable models, followed by a discussion of their biological assumptions. Finally, the scenario of a non-homogenous mussel distribution is investigated in chapter (10). It turns out that even heap-like mussel accumulations on the seabed evoke similar wavelike starfish invasions as in the model with homogenous mussel distribution studied in the chapters before.

2 Biological background on starfish and mussels in the Limfjord

In this chapter, the biological background for the model will be presented. It consists of basic information about the Limfjord as well as starfish and mussel behaviour, as far as it is relevant to this master thesis.

2.1 Limfjord

The Limfjord is a 180 km sea arm in Denmark, separating Jutland peninsula and the island of Vendsyssel-Thy. It connects the North Sea with the Kattegat (sea between Denmark and Sweden) and consists of salty, shallow water at a maximum depth of 24m. The connection between the two seas was created in 1825, when the North Sea broke through from the west. Nowadays, the channel is kept open artificially. The region is famous for its tasty mussels and oysters. However, starfish invasions are a serious threat to mussel beds, because they are able to erase whole areas of mussels (cf. Saier (2001)). Thus, it is of great interest to know the starfish and mussel distribution in Limfjord. Research on mussels and shellfish in general as well as regular counting at selected positions in the Limfjord is done by the Dansk Skaldyrcenter (DSC, Danish shellfish center)[1] located in Nykøbing Mors, cf. figure (2).

2.2 Mussels[2]

The most common mussel in Denmark and also in the Limfjord is the blue mussel (*Mytilus edulis*). It is an eatable mussel, which lives up to 8 years in dense mussel beds on the sea bed. Those mussel beds cover the sea bed in some parts like a carpet. They mostly occur in a depth up to 10 meters. Recently, it has been managed to breed blue mussels on ropes. This gives an additional possibility to harvest mussels from the sea bed and thus increase the mussel production in the Limfjord.
Blue mussels are filter feeders, which means that they filter sea water to feed on plankton. As most mussels, they have no means to move or approach food and are therefore highly dependent on the water current.

[1] www.skaldyrcenter.dk

[2] The information in this paragraph is based on: `http://e-learning.skaldyrcenter.dk/produkter/blaamusling/`, an e-learning platform by the Danish shellfish center (in Danish)

Figure 2: DSC's research vessel at the Limfjord, Nykøbing Mors

The blue mussels' natural enemies are crabs, birds and starfish, which can open a mussel with their arms before they digest them with their mouth.

2.3 Starfish[3]

The most common starfish in Denmark is *Asterias rubens*, which can reach a size of up to 30cm and an age of up to 8 years. They usually have five tube feet and a mouth based in the lower center of the body. Although they also eat sea urchins and various other small organisms, their main nutrition is mussels.

It has been reported in different areas of the world that starfish form wave-like feeding fronts on the sea bed, when they exploit a mussel bed, e.g. Lauzon-Guay et al. (2008) at St. Croix, U.S. Virgin Islands (cf. figure (1)) or Dare (1982) at Moracambe Bay, Irish Sea. This is especially remarkable, since starfish are considered by biologists to be solitary and not communicating with each other.

[3] The information in this paragraph is based on: `http://e-learning.skaldyrcenter.dk/produkter/soestjerne/`, an e-learning platform by the Danish shellfish center (in Danish)

Figure 3: Starfish on DSC's research vessel, Limfjord

2.4 Starfish feeding on mussels

Mussels are very limited in their movement. This means that they can be seen as static in contrast to the starfish predating on them. A characteristic feature of predator-prey relationships as between starfish and mussels is the question of kinesis, taxis and chemotaxis. These terms describe the way how the predator approaches the prey. While kinesis means an organism's non-directional reaction to a stimulus, taxis is a directional movement due to a stimulus like presence of food. If the stimulus is chemical, it is called chemotaxis. Up to now, there is no evidence that starfish are able to detect mussels over a distance. Thus, their movement in absence of prey can be assumed as unbiased random walk. As soon as they reach a mussel bed, they slow down and stop to clasp a mussel. After cracking it open and digesting it through the protruded stomach, it takes some time until the starfish is ready to resume its movement.
A detailed study about Asteria rubens L. starfish attacking Mytilus edulis L. mussels can be found in Norberg and Tedengren (1995).

3 Spatial patterns in PDE

This chapter will briefly introduce the concept of pattern forming solutions to PDE (partial differential equations) as well as basic definitions and concepts used in this master thesis.

A partial differential equation is defined as an equation in an unknown function u in several variables and its partial derivatives. Let Ω be a domain and $u : \Omega \subset \mathbb{R}^n \to \mathbb{R}$. In this thesis, we will focus on functions in $n-1$ spatial variables $x = (x_1, ..., x_{n-1})$ and one time variable t.

In the models used for the numerical simulation $n = 2$. Hence, there is only a one-dimentional spatial variable x and one time variable t. For the partial derivatives, the following abbreviations might be used in certain equations to simplify the notation:

$$u'(x,t) \coloneqq \frac{\partial u}{\partial x}(x,t) \tag{1}$$

$$\dot{u}(x,t) \coloneqq \frac{\partial u}{\partial t}(x,t) \tag{2}$$

3.1 Traveling wave solutions

For mathematical models in biology it is often of particular interest to consider pattern-forming solutions to PDE, e.g. epidemic waves or invasion waves. In these cases, a sudden change in animal numbers evolves in a certain region at a certain speed. This could be a new species invading a former uninhabited area or an epidemic spreading in a population of healthy individuals. Numerous examples can be found in Shigesada and Kawasaki (1997) or Murray (2003) for example.

One standard concept to describe these phenomena are traveling waves:

Definition 1. *Traveling wave (solution):*
A solution $u(z)$ to a PDE in $u(x,t)$ with $z \coloneqq x - ct$ or $z \coloneqq x + ct$.

Traveling wave solutions preserve their shape over time and move at constant velocity c. However, they exist only for few partial differential equations. A famous equation allowing a traveling wave solution is the wave equation, a linear hyperbolic PDE:

$$c^2 \Delta u = u_{tt} \tag{3}$$

The classical solution to this equation for $x \in \mathbb{R}$ and $t \geqslant 0$ can be written as:

$$u(x,t) = \frac{1}{2}(u_0(x-ct) + u_0(x+ct)) + \frac{1}{2c}\int_{x-ct}^{x+ct} u_1(z)\,dz \tag{4}$$

Here $u_0 = u(.,0)$ and $u_1 = u_t(.,0)$ denote the initial values of the function $u(x,t)$ and its derivative $u_t(x,t)$.
Further, the term invasion wave will be used to describe the entry of the starfish population into a new territory. This means that in front of the traveling wave, there are no starfish present.

Definition 2. *Invasion wave:*
A traveling wave solution $u(z)$ to a PDE in $u(x,t)$ with $\lim_{z\to\infty} u(z) = 0$

3.2 Diffusion equation

The diffusion equation, also called heat equation, is a linear parabolic PDE:

$$u_t = D\,\Delta u \tag{5}$$

In this equation, D denotes the diffusivity and is a measure for the spatial spread of the population $u(x,t)$ over time t. In this scenario diffusivity is constant, which means that no outer effects influence the population's movement.
It can be proven, that for a pure diffusion equation, there cannot be traveling waves (cf. Murray (2003), p. 438f). For simplicity, the calculations are done with a one-dimensional space-coordinate.
The traveling wave ansatz $z = x - ct$ yields by application of the chain rule:

$$\frac{du}{dz} = \frac{\partial u}{\partial x}\frac{\partial x}{\partial z} + \frac{\partial u}{\partial t}\frac{\partial t}{\partial z} \tag{6}$$

$$= \frac{\partial u}{\partial x} - \frac{1}{c}\frac{\partial u}{\partial t} \tag{7}$$

Inserting this equation into the diffusion equation yields an ODE (ordinary differential equation) for $u(z)$:

$$-c\frac{du}{dz} = D\frac{d^2u}{dz^2} \tag{8}$$

$$D\frac{d^2u}{dz^2} + c\frac{du}{dz} = 0 \tag{9}$$

The solution to this system is $u(z) = A + Be^{\frac{-cz}{D}}$. For $B \neq 0$ the limit $\lim_{z\to-\infty} u(z)$ becomes unbounded. Thus, $B = 0$ and the traveling wave solution is actually a constant function. This means that a pure diffusion equation is not able to model traveling wave behaviour of a population. One possible adaption is to include population growth in the form of a function $f(u)$ into the model:

$$u_t = f(u) + D\,\Delta u \tag{10}$$

The function $f(u)$ could refer to logistic growth or exponential growth or a natural death process. Depending on the function $f(u)$ there might exist traveling wave solutions or not (cf. Shigesada and Kawasaki (1997), p. 48).

3.3 Advection-diffusion equation

The advection-diffusion equation, also named Fokker-Planck or Fisher-Kolmogorov equation, is an extension to the pure diffusion equation by considering variations of the diffusivity $D(x,t)$ depending on space and time. This is a common assumption for many biological situations, e.g. a predator's movement depending on the presence of prey or an epidemic's spread depending on the presence of susceptible individuals. All these scenarios can be modeled by an advection-diffusion equation, where $D = D(x,t)$:

$$u_t = \Delta(Du) \tag{11}$$

It can be shown, that for this equation actually exist traveling wave solutions (cf. Murray (2003), chapter 13.2, 13.4.).

The advection-diffusion equation can be derived from a random walk model (cf. Shigesada and Kawasaki (1997), p. 56 or Murray (2001)). In contrast to the diffusion equation, which is based on an unbiased random walk, the advection-diffusion equation is based on a biased random walk. This bias is due to the advective flux.

From an Itō calculus point of view the advection-diffusion equation is also called Kolmogorov forward equation. An Itō process in one spatial dimension X_t with diffusion $D(X_t,t)$ and drift $\mu(X_t,t)$ is defined by the SDE (stochastic differential equation)

$$dX_t = \mu(X_t,t)\,dt + \sqrt{2D(X_t,t)}\,dB_t \tag{12}$$

Then the Kolmogorov forward equation for the probability density function $\varphi(x,t)$ of X_t

corresponds to an advection-diffusion equation:

$$\frac{\partial \varphi(x,t)}{\partial t} = -\frac{\partial}{\partial x}\left[\mu(x,t)\varphi(x,t)\right] + \frac{\partial^2}{\partial x^2}\left[D(x,t)\varphi(x,t)\right] \tag{13}$$

This equation describes how probability will be redistributed in space by means of the advective and diffusive transport. Thus, the equation governs the probability density of the state X_t as a function of time, when the initial condition is a random variable. Further information on the connection between advection-diffusion equations and SDE can be found in Gardiner (2002).

3.4 Conclusion

Those results about different PDE will be used to develop a model for starfish feeding on mussels, which allows wave like solutions. Since Fickian diffusion alone is not able to form traveling waves, an advection-diffusion approach is a reasonable choice. The numerical results presented in chapter (5) and the analytical results presented in chapter (7) show that an advection-diffusion equation in combination with a harvesting equation can actually result in wavelike solutions. Depending on the model details, such as the harvesting function, the diffusivity function or initial conditions, those might be traveling wave solutions in a classical sense or other wavelike phenomena.
Thus, it is worth mentioning that traveling waves in the classical sense are not the only wave phenomena occurring in PDE. Campos et al. (2013) describe discontinuous traveling waves, which they call entropy solutions, in an article on reaction-diffusion equations.

4 Advection-diffusion model without mussel growth

In this chapter, the specific model, which was used to describe the starfish propagation and the mussel abundance based on the biological conditions in the Limfjord (cf. chapter (2)), will be introduced and explained. The essential model requirement was the ability to describe a wavelike starfish feeding front movement, while keeping assumptions on the animals' behaviour as low as possible.

4.1 Biological assumptions

The biological situation in the Limfjord as well as the characteristic behaviour of mussels and starfish were briefly explained in chapter (2). This makes the following assumptions reasonable:

1. The starfish have no means to detect mussels from a distance and move randomly and unbiased on the seabed at constant velocity.[4] They are not subject to drift. Thus, the starfish density $S(x,t)$ at a specific point x at time t is subject to a diffusion process.

2. As soon as the starfish reach a position with positive mussel density $M(x,t)$, they start feeding on them and slow down their movement. Thus, the starfish diffusivity function $D = D(M(x))$. It is reasonable to assume this function D to be a monotonically decreasing continuous function $\overline{\mathbb{R}^+} \to \overline{\mathbb{R}^+}$.

3. The mussel density $M(x,t)$ at a specific point x and time t is not subject to diffusivity, because in comparison to the starfish velocity, the mussel movement can be neglected.

4. Mussel growth is very slow in comparison to the system dynamics and will be neglected for a start. Thus, the mussel density only changes because of the starfish's harvesting. The harvesting rate $h(M(x,t))$ per unit starfish density only depends on the mussel density. Again, it is reasonable to assume the function $h(M(x,t))$ to be a monotonically increasing continuous function from $\overline{\mathbb{R}^+} \to \overline{\mathbb{R}^+}$.

[4] In terms of SDE (stochastic differential equations): Starfish movement is a martingale. This means that one specific starfish's position is a stochastic process (=sequence of random variables). At any time in the realized sequence, the expectation of the next value is equal to the present observed value.

4.2 Mathematical description and derivation of a dimensionless system

In chapter (3), it was already mentioned that a diffusion equation does not allow traveling wave solutions. Thus, it is necessary to use an advection-diffusion equation for the starfish movement, i.e. a non-constant diffusivity function. The upper assumptions yield the following advection-diffusion model to describe the starfish S and mussel M distribution with a diffusivity function $\widetilde{D}$ and harvesting function $\widetilde{h}$:

$$\frac{\partial}{\partial \widetilde{t}}\widetilde{S} = \frac{\partial^2}{\partial \widetilde{x}^2}(\widetilde{D}(\widetilde{M})\widetilde{S}) \tag{14}$$

$$\frac{\partial}{\partial \widetilde{t}}\widetilde{M} = -\widetilde{h}(\widetilde{M})\widetilde{S} \tag{15}$$

In this system, there are four quantities subject to scaling: space $\widetilde{x}$, time $\widetilde{t}$, starfish abundance $\widetilde{S}$ and mussel abundance $\widetilde{M}$. It can be shown that scaling does not influence the model and the results. When starting with a system subject to scaling it is always possible to redefine the variables to obtain a dimensionless system of the same shape. This will be carried out with non-zero scaling factors M^*, S^*, x^*, t^* and the substitutions:

$$S = \frac{\widetilde{S}}{S^*} \tag{16}$$

$$M = \frac{\widetilde{M}}{M^*} \tag{17}$$

$$t = \frac{\widetilde{t}}{t^*} \tag{18}$$

$$x = \frac{\widetilde{x}}{x^*} \tag{19}$$

Substituting in equation (14) yields an equation for $D(M)$, the dimensionless diffusivity function:

$$\frac{\partial}{\partial t}S = \frac{t^*}{S^*}\frac{\partial \widetilde{S}}{\partial \widetilde{t}} = \frac{t^*}{S^*}\frac{\partial}{\partial \widetilde{x}^2}\left(\widetilde{D}(\widetilde{M})\widetilde{S}\right) = \frac{t^*}{S^*}x^*\frac{\partial}{\partial x^2}\left(\widetilde{D}(M^*M)S^*S\right) \stackrel{!}{=} \frac{\partial}{\partial x^2}(DS) \tag{20}$$

This yields a diffusivity function $D(M)$ for the dimensionless system:

$$D(M) = t^*x^*\widetilde{D}(M^*M) \tag{21}$$

The same procedure for equation (15) yields an equation governing the dimensionless harvesting function $h(M)$:

$$\frac{\partial}{\partial t}M = \frac{t^*}{M^*}\frac{\partial \widetilde{M}}{\partial \widetilde{t}} = -\frac{t^*}{M^*}\widetilde{h}(\widetilde{M})\widetilde{S} = -\frac{t^*}{M^*}\widetilde{h}(M^*M)\widetilde{S}^*S \stackrel{!}{=} -h(M)S \tag{22}$$

This yields a harvesting function for the dimensionless system:

$$h(M) = \frac{S^*t^*}{M^*}\widetilde{h}(M^*M) \tag{23}$$

From now on, the dimensionless model will be used for further analysis. This model is a PDE system of second order:

$$\boxed{\begin{aligned}\frac{\partial S(x,t)}{\partial t} &= \frac{\partial^2}{\partial x^2}\left[D(M(x,t))S(x,t)\right] \\ \frac{\partial M(x,t)}{\partial t} &= -\,h(M(x,t))S(x,t)\end{aligned}}$$

The calculations in this section show that it is possible to choose the characteristic scales (M^*, S^*, x^*, t^*) at will to obtain simplifications in the PDE system. For example could it be desirable for comparison to other scientists' results or for reasons of simplicity in the calculations to have e.g. $M(x,0) = 1$ before the starfish invasion or the diffusivity respectively harvesting function should have a specific value at a specific point, e.g. $D(1) = 1$ and $h(1) = 1$. This can be achieved by inserting the values $\widetilde{D}(1)$ and $\widetilde{h}(1)$ into the equations (21) and (22) and appropriate choices of the scales (M^*, S^*, x^*, t^*) to satisfy them.

5 Simulation of an advection-diffusion model without mussel growth

This chapter describes the numerical simulations of the advection-diffusion model without mussel growth introduced in chapter (4):

$$\frac{\partial S(x,t)}{\partial t} = \frac{\partial^2}{\partial x^2}\left[D(M(x,t))S(x,t)\right] \tag{24}$$

$$\frac{\partial M(x,t)}{\partial t} = -h(M(x,t))S(x,t) \tag{25}$$

The numerical simulation was implemented in Matlab (version 2014a). The aim was to collect information on the starfish propagation for a detailed analysis (cf. chapter (6)). The plots of the functions used in the model were done with Maple 17.

5.1 General parameters

The spatial domain of the simulation is one dimensional and consists of the interval $[0, L] \subset \overline{\mathbb{R}^+}$. The length of the domain is $L = 50$, with a number of 250 evenly spread grid cells on it. Thus, each grid cell has a length of 0.2 units. In each grid cell, there is a starfish density $S(x,t)$ and mussel density $M(x,t)$ located in the middle of the cell. The changes in those densities are governed by the PDE system, which is solved numerically.

5.2 Numerical methods

This section will give further details on the numerical methods used in the algorithm. As usual for finite volume methods, the interval $[0, L]$ was divided into equally spaced subintervals. These are typically called volumes. Every one of them is represented by an interior point, in this simulation it was the center point. As a primary method to solve the PDE system, the method of lines (MOL) was used. The method of lines is a numerical procedure to solve time dependent partial differential equation systems such as the advection-diffusion model presented in this thesis. The idea is to discretize all variables except one and solve the resulting ODE system with a standard method (e.g. Runge-Kutta). Detailed information on MOL can be found in Schiesser (1991) or Hamid et al. (2007). In the simulations carried out for this thesis, the unknown spatial derivatives were approximated by first order finite difference quotients. By taking into account the direction of flow, a so-called upwind approach, one can overcome issues of

other differencing schemes. The procedure of discretizing the spatial variable yields an ODE system with the time t as the only continuous and independent variable. To solve this system a standard Matlab odesolver, i.e. ode45, was applied.
An important property of this approach is the fact that mass will be conserved. Thus, it is secured that a probability density function (pdf) as initial condition can still be interpreted as a pdf at all later times of the simulation.

5.3 Algorithm to solve the PDE system

In every time step an ODE system was solved with the Matlab odesolver ode45, a Runge-Kutta method, and 1e-3 tolerance to keep computation time in an acceptable time frame. To make the algorithm better understandable, the starfish equation will be rewritten in advection-diffusion form:

$$\frac{\partial S}{\partial t} = (DS)'' \tag{26}$$

$$= (D'S + DS')' \tag{27}$$

$$= -\frac{\partial}{\partial x}\left(- \underbrace{D'S}_{\text{advective flux}} \underbrace{-DS'}_{\text{diffusive flux}} \right) \tag{28}$$

$$\tag{29}$$

For each time step t the following calculations are executed to obtain the vector of derivatives $\frac{dM(x)}{dt}$ and $\frac{dS(x)}{dt}$, which are later used by the odesolver ode45, an explicit Runge-Kutta (4,5) method. Since computing a new value only requires the solution at the immediately preceding time point, it is a one-step solver.
In this subsection expressions such as $\frac{\Delta M}{\Delta x}$ always denote the forward difference quotient:

$$\frac{\Delta M(x_i)}{\Delta x} = \frac{M(x_{i+1}) - M(x_i)}{x_{i+1} - x_i} \tag{30}$$

For each grid cell x_i the following steps are executed:

1. Transport of the starfish:

   a) Compute the advective flux $J_a(x_i)$ by using $D' = \frac{\partial D}{\partial M}\frac{\partial M}{\partial x}$. While $\frac{\partial D}{\partial M}$ is known,

$\frac{\partial M}{\partial x}$ needs to be approximated by a difference quotient:

$$J_a(x_i) = -\frac{\partial D}{\partial M}(x_i)\frac{\Delta M(x_i)}{\Delta x_i}S(x_i) \tag{31}$$

If $\frac{\partial D}{\partial M}(x_i)\frac{\Delta M(x_i)}{\Delta x_i}$ is negative, the direction of transport is reversed and instead of $S(x_i)$, it is necessary to use $S(x_{i+1})$.

b) Compute the total flux $J(x_i) = J_a(x_i) + J_d(x_i)$ as sum of the advective $J_a(x_i)$ and the diffusive flux $J_d(x_i)$ by approximating $S'(x_i)$ with the difference quotient $\frac{\Delta S(x_i)}{\Delta x_i} = \frac{S(x_{i+1})-S(x_i)}{x_{i+1}-x_i}$:

$$J(x_i) = J_a(x_i) + J_d(x_i) = J_a(x_i) - D\left(M(x_i)\right)\frac{\Delta S(x_i)}{\Delta x_i} \tag{32}$$

c) Update

$$\frac{dS(x_i)}{dt} = \frac{dS(x_i)}{dt} - \frac{\Delta J(x_i)}{\Delta x_i} \tag{33}$$

2. Mussel harvest:

$$\frac{dM(x_i)}{dt} = -h(M(x_i))S(x_i) \tag{34}$$

Since the grid is a bounded interval $[0, 50]$, it is necessary to define boundary conditions. In this simulation the boundary conditions were set to be reflective. This means the starfish change direction and stay in the defined area instead of crossing the interval's boundary. Thus, there is no starfish flux across the boundaries.

5.4 Diffusivity & harvesting function

5.4.1 Diffusivity function

As diffusivity function $D_k(M)$, a sigmoid function with parameter $k > 0$ was chosen:

$$D_k(M) = 1 - \frac{1}{1+\exp(-kM)} = \frac{1}{1+\exp(kM)} \tag{35}$$

The reason to choose this specific function is due to the fact that it has all the necessary properties for a diffusivity function, which are summarized as follows:

1. This function is C^∞ on $\mathbb{R}$, in particular the first and second derivative exist on $\mathbb{R}^+$ and can thus be used to compute the flux between the grid cells.

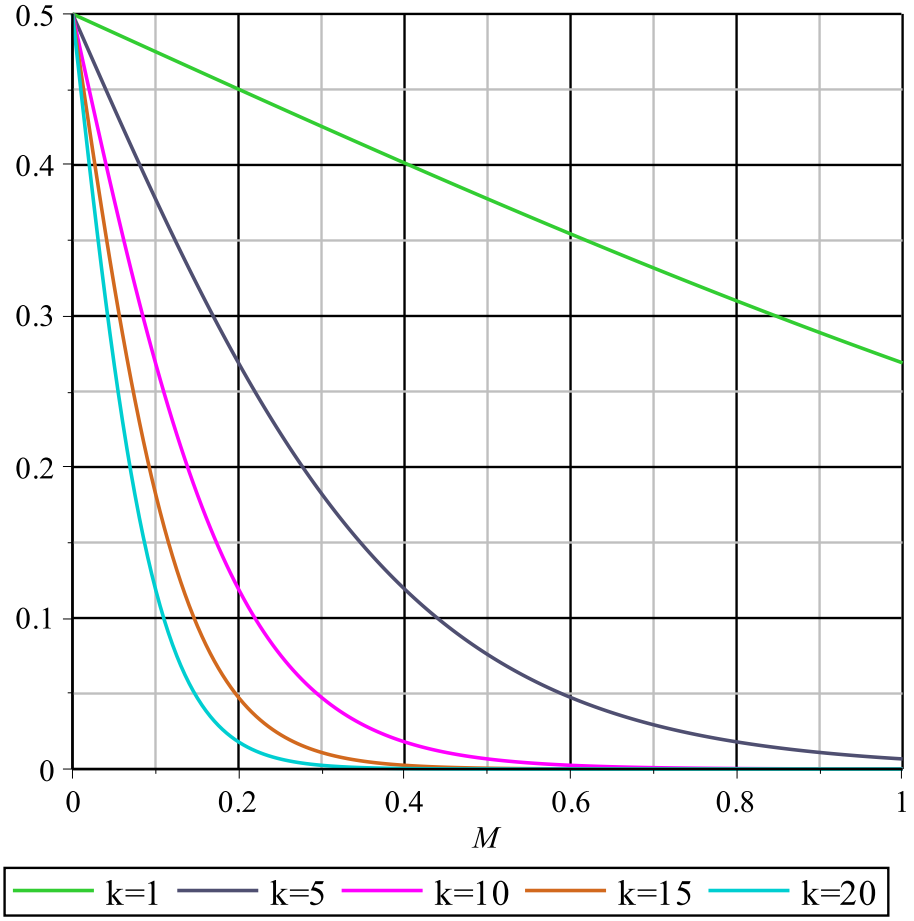

Figure 4: Diffusivity function $D(M) = 1 - \frac{1}{1+e^{-kM}}$ for $k \in \{1, 5, 10, 15, 20\}$

2. The function's image is always in the interval $[0, \frac{1}{2}]$ and hence non-negative.

3. The parameter k makes it possible to vary between different types of functions, cf. figure (4). For large k, we obtain a function, which imitates a step function as used in a model by Abraham (2007), cf. chapter (9.1). This parameter choice indicates, that starfish stop moving and start feeding immediately, as soon as there is a positive mussel density. For small k, the diffusivity function becomes less ambivalent and more linear on the interval $[0, 1]$. As soon as there are mussels available, the starfish gradually slow down, but won't come to a halt immediately.

   For all $M \in \mathbb{R}^+$ holds:

$$\lim_{k \to \infty} D_k(M) \searrow 0 \tag{36}$$

   For $M = 0$ holds for all $k \in \overline{\mathbb{R}^+}$:

$$D_k(0) = \frac{1}{2} \tag{37}$$

5.4.2 Harvesting function

Mussel decline happens solely due to the starfish feeding on them. A predator's intake rate as a function of prey density is called *functional response*. Holling (1959) classified three types of functional responses, cf. figure (5). A detailed explanation can be found in Begon et al. (2006).

1. Type I: The relation between prey density and harvesting rate is a linear function.

2. Type II: No matter low or high prey densities, the harvesting rate grows less than a linear function.

3. Type III: For low prey densities, the harvesting rate grows more than a linear function, but later slows down by growing less than a linear function.

The type II functional response was first described by Holling (1959). In an experiment he let a blindfolded assistant harvest discs from a table. Holling observed that the amount of harvested prey was decelerating for higher prey densities. His explanation was, that a larger density implies relatively more time spent on feeding than on actively searching. The following equation models this scenario:

$$y = \frac{Tax}{1 + abx} \tag{38}$$

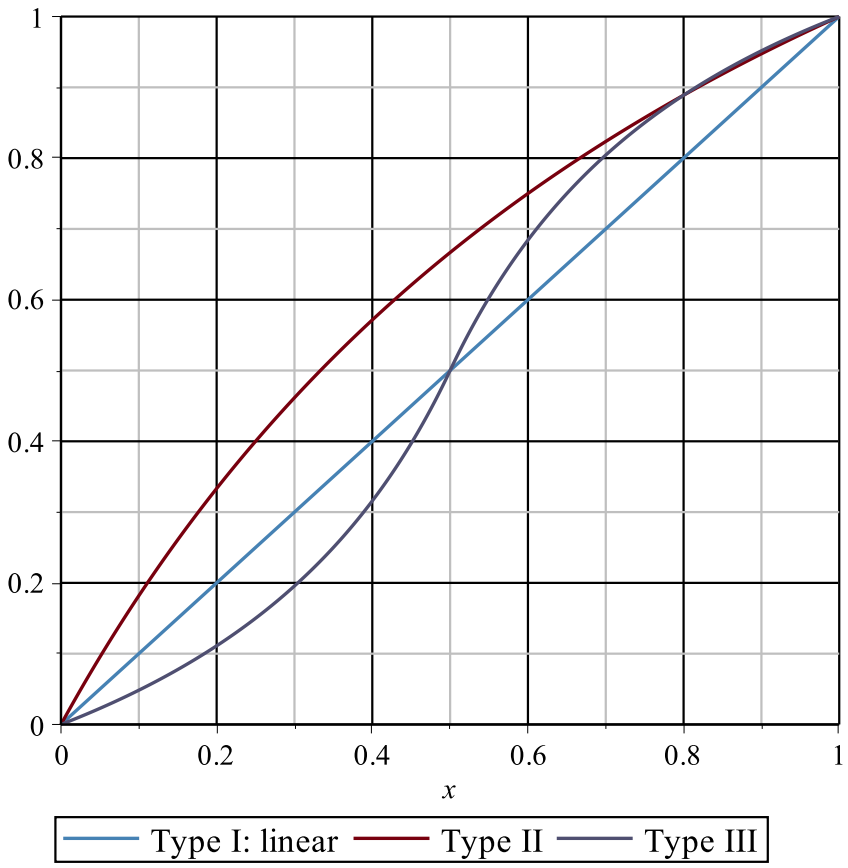

Figure 5: Functional response type I, type II and type III

The variable x denotes the prey density and y the harvesting rate. Parameter T is the available time frame, b is the time it takes to pick up one unit of prey and a the discovery rate.

Begon et al. (2006) give a detailed explanation of type II functional responses on page 308:

> The type 2 response can be explained by noting that a predator has to devote a certain handling time to each prey item it consumes (i.e. pursuing, subduing and consuming the prey item, and then preparing itself for further search). As prey density increases, finding prey becomes increasingly easy. Handling a prey item, however, still takes the same length of time, and handling overall therefore takes up an increasing proportion of the predator's time - until at high prey densities the predator is effectively spending all of its time handling prey. The consumption rate therefore approaches and then reaches a maximum (the plateau), determined by the maximum number of handling times that can be fitted into the total time available.

The situation in Holling's experiment can be compared to the starfish looking for mussels on the seabed, since starfish have no means to percept mussels from a distance. Besides, it takes starfish some time to actually open, eat and digest a mussel, which corresponds to the scenario Begon et. al. describe. Thus, a Holling type II functional response was chosen for the simulations (cf. figure (6)).[5]

$$h(M(x,t)) = \frac{M(x,t)}{M(x,t)+1} \tag{39}$$

This strictly monotonic increasing function crosses the origin and reaches a maximum of 0.5 on the interval $[0,1]$ for $M = 1$. This means that the more mussels there are available, the less the harvesting rate increases. The half-saturation constant for the harvesting is 1, as well as the maximal grazing rate per starfish. The maximal grazing rate is defined as the limit of the harvest function:

$$\lim_{M\to\infty} h(M) = \lim_{M\to\infty} \frac{M}{M+1} = 1 \tag{40}$$

[5] Sometimes, this type of functional response is also called Michaelis-Menten kinetics.

The half-saturation constant is defined as the mussel density M at half of the harvesting function's maximum:

$$M\left(\frac{1}{2}\lim_{M\to\infty} h(M)\right) = M\left(\frac{1}{2}\right) = 1 \tag{41}$$

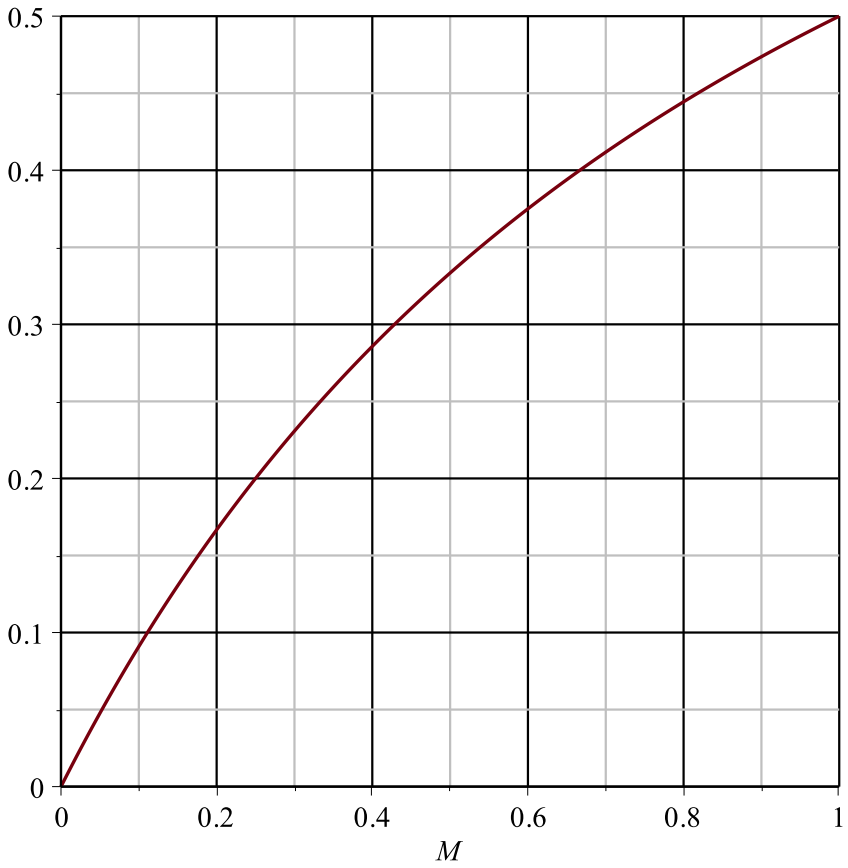

Figure 6: Functional response Holling type II used in the simulation: $h(M) = \frac{M}{1+M}$

5.5 Initial conditions

The initial mussel density in the whole domain $[0, 50]$ was set to 1. This is consistent with a homogenous mussel distribution on a short section of an "infinite" sea bed. The initial starfish distribution follows a scaled normal distribution with parameters $\sigma^2 = \frac{25}{2}$ and $\mu = 0$ on the interval $[0, 50]$ (cf. figure (7)):

$$S(x,0) = \frac{1}{\int_0^{50} \exp\left(\frac{-x^2}{5^2}\right)\, dx} \exp\left(\frac{-x^2}{5^2}\right) \tag{42}$$

$$= 2\frac{1}{\sqrt{2\pi\frac{25}{2}}} \exp\left(-\frac{x^2}{5^2}\right) \tag{43}$$

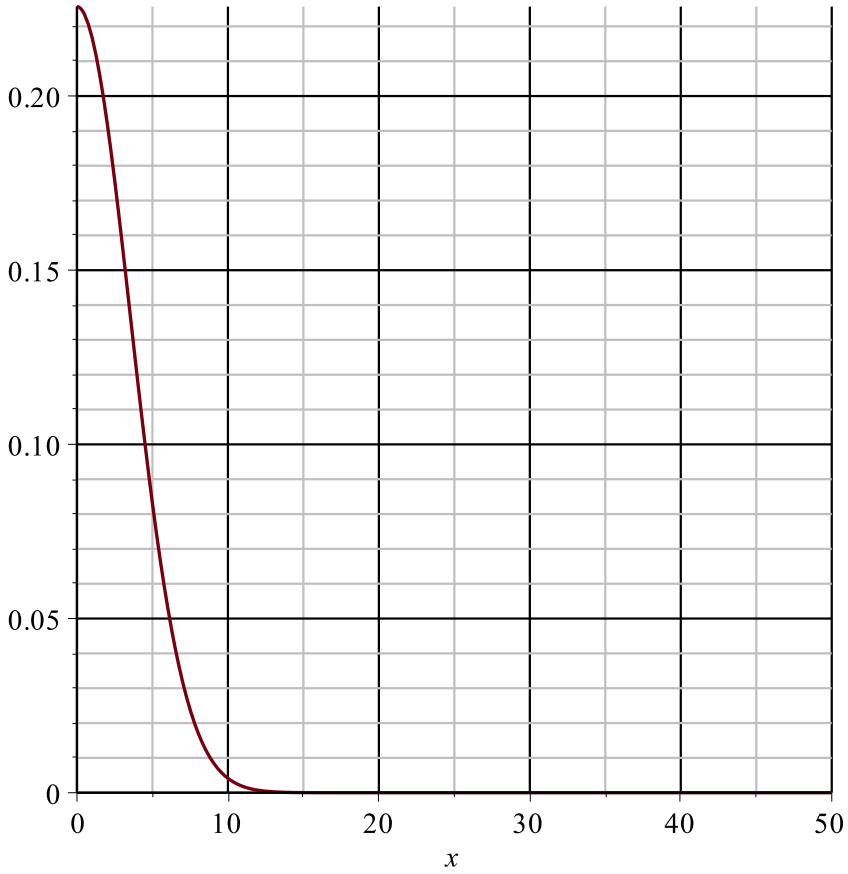

Figure 7: Initial starfish abundance on the interval $[0, 50]$: $S(x,0) = \frac{1}{\int_0^{50} \exp\left(\frac{-x^2}{5^2}\right) dx} \exp\left(\frac{-x^2}{5^2}\right)$

This is consistent with a Gaußian-like starfish invasion entering the domain at the point $x = 0$.

5.6 Heatmaps

All the heatmaps in this master thesis have the same properties. The upper figure is always showing the starfish density $S(x,t)$, the lower figure the mussel density $M(x,t)$.

The x-axis denotes time t, while the y-axis denotes the sea bed, i.e. space on the interval $[0, 50]$. The colouring visualizes the starfish and mussel density, red meaning high concentration and blue low concentration.

5.7 Diffusivity function parameter variation

This section will depict how changes in the diffusivity function affect starfish and mussel densities in the model. The aim is to point out differences due to the variation of parameter k. A more profound analysis of the model dynamics is done in the subsequent chapter. Figure (4) shows the diffusivity functions for $k \in \{1, 5, 10, 15, 20\}$. Parameter $k = 1$ gives a decreasing almost linear function on $[0, 1]$. This corresponds to a situation, where the starfish movement depends linearly on mussel density. The other cases $k \in \{5, 10, 15, 20\}$ describe a scenario, where starfish slow down quite fast, as soon as there is prey available. However, their speed changes no longer much, as soon as a certain level of mussels is present. The following figures (8), (9), (10), (11), (12) show a comparison between different values of k.

5.7.1 Wavelike behaviour: shape & width

The first striking pattern is the wavelike starfish invasion moving from $x = 0$ to $x = 50$, which is visualized in the upper heatmaps. A clear front separates the former uninhabited area (dark blue) from the invaded area (light blue). At the same time, the mussel bed (red) in the lower heatmaps is harvested in a sharp front, which displays a wave traveling from $x = 0$ to $x = 50$, no matter which value the parameter $k \in \{5, 10, 15, 20\}$ assumes. Both wavefronts form already after a very short time frame (t = 100) and thus quite fast in comparison to the total grazing time of several thousand time steps (cf. section 5.7.2). For parameters $k = 1$ (figure (8)) and $k = 5$ (figure (9)) the starfish front as well as the mussel front move in an almost linear way. This means the wavefronts move at a constant speed following a power law of $\approx t^1$. The heatmaps for parameters $k = 10$ (figure (10)), $k = 15$ (figure (11)) and $k = 20$ (figure (12)) show that the fronts' moving speed is actually slowing down over time. Thus, the behaviour is no longer linear, but a power law of order > 1. A detailed analysis of this relation is done in the subsequent chapter (6). While for parameter $k = 1$ the mussel front still shows a relatively broad width (red-yellow-green-light blue), the higher parameter values $k = 10$ (figure (10)), $k = 15$ (figure (11)) and $k = 20$ (figure (12)) yield a low front width (strict separation between the untouched mussel bed in red and the harvested one in blue) and thus an

even clearer wavefront.

5.7.2 Grazing speed & time

It becomes evident that for increasing parameter k the starfish need more and more time to erase the mussel bed. While for $k \leqslant 5$ it takes the starfish population only up to 1000 time steps to erase the whole mussel population, it is about 9000 time steps for $k = 20$. This is plausible, because equation (36) states that increasing k slows down the diffusion process and thus starfish progression.

5.7.3 Peaks in the population density

For parameter $k = 1$, the upper plot in figure (8) shows no clear front between the invaded and the not yet invaded area from a starfish point of view. This means, starfish diffusion is not much affected by the presence or lack of mussels and is consistent with the only slowly decreasing function $D_1(M) = 1 - \frac{1}{1+\exp(-M)}$ on the interval $M \in [0, 1]$. Neither is there a sharp and clear border separating the intact from the harvested mussel bed in figure (8), with parameter $k = 1$. However, for the larger parameters, the evident red-blue partitioning in the lower plot proves the existence of such a sharp boundary in the mussel bed (cf. figures (9), (10), (11), (12)).

5.8 Conclusion

The simulations of the advection-diffusion PDE model with varying diffusivity function parameter k yielded basically similar results. Naturally, there are differences in grazing speed and time, but the system's dynamic remains unchanged. For increasing parameter k, the starfish wavefront becomes clearer and sharper and follows a powerlaw of order > 1. This corresponds to a steeper diffusivity function. Especially, the wavefront's propagation speed and shape are of high interest. Thus, the following chapter will further investigate and characterize the wavelike solutions obtained in the numerical simulations.

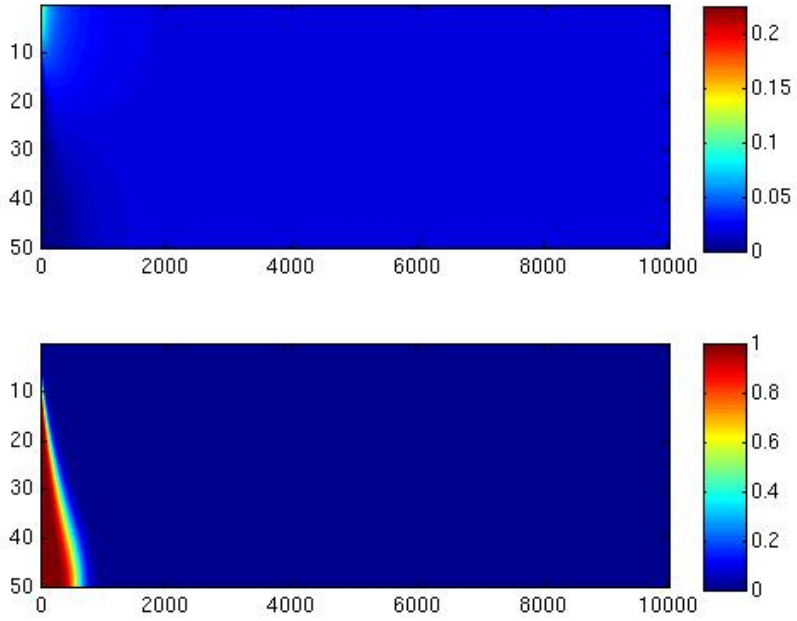

Figure 8: Starfish and mussel density with diffusivity function $D(M) = 1 - \frac{1}{1+e^{-kM}}$, $k = 1$

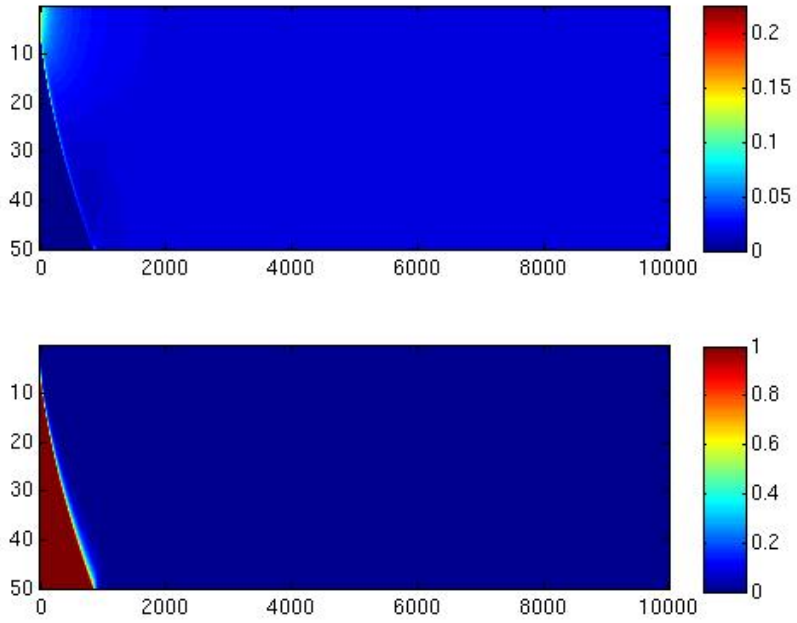

Figure 9: Starfish and mussel density with diffusivity function $D(M) = 1 - \frac{1}{1+e^{-kM}}$, $k = 5$

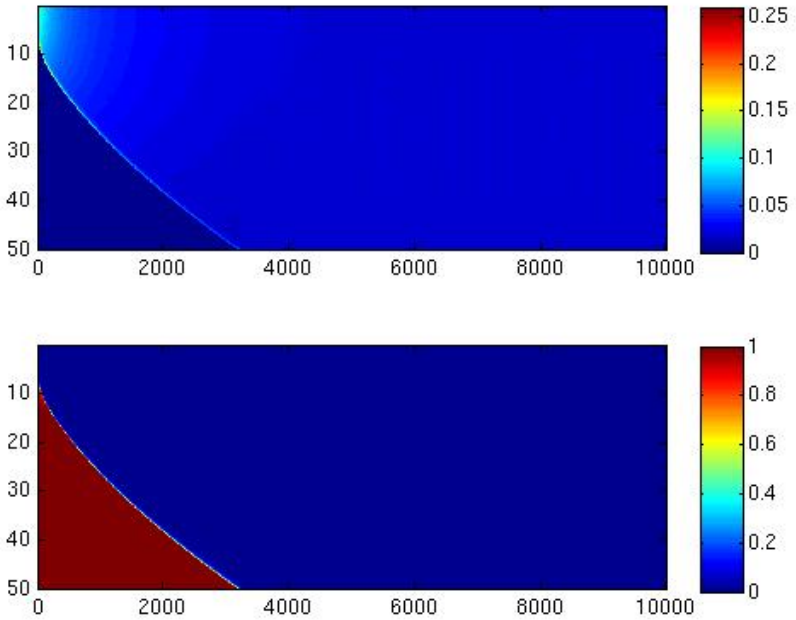

Figure 10: Starfish and mussel density with diffusivity function $D(M) = 1 - \frac{1}{1+e^{-kM}}$, $k = 10$

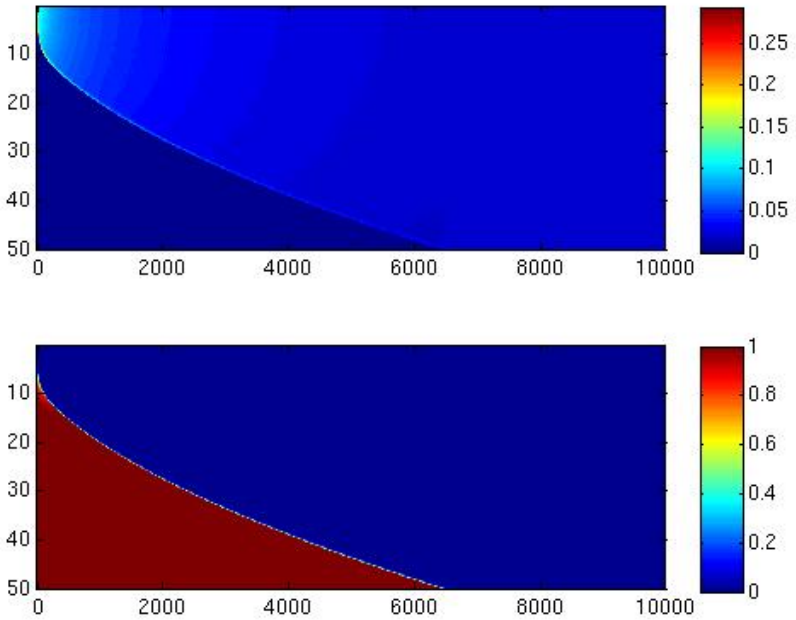

Figure 11: Starfish and mussel density with diffusivity function $D(M) = 1 - \frac{1}{1+e^{-kM}}$, $k = 15$

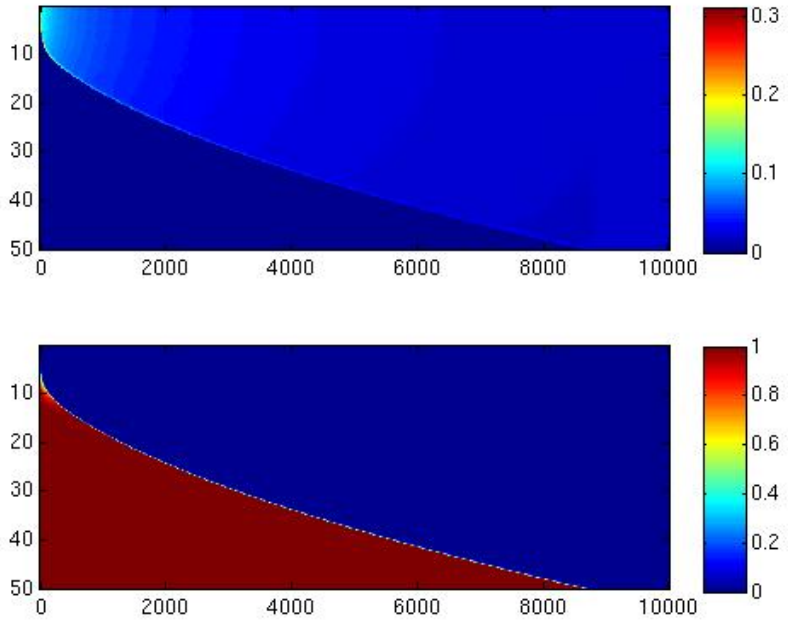

Figure 12: Starfish and mussel density with diffusivity function $D(M) = 1 - \frac{1}{1+e^{-kM}}$, $k = 20$

6 Characterising numerical solutions of an advection-diffusion model without mussel growth

This chapter will present a detailed analysis of the data obtained in the simulations in chapter (5). Of special interest is a characterization of the wavefronts in terms of shape, speed and amplitude. Figure (12) with $k = 20$ seems to capture the underlying system dynamics in a sufficient way, because it displays the starfish and mussel wavefronts sharply and clearly. Besides, the wavefronts' shapes do no longer change characteristically in contrast to $k = 10$ or $k = 15$. Hence, figure (12) and $k = 20$ will be used for a thorough analysis of the changes in the mussel and starfish density. On the other hand the diffusivity function with $k = 20$ is still far from approximating a step function and hence a reasonable choice from a biological point of view, cf. section (9.3).
As already mentioned, the plots show the starfish and mussel density in the spatial interval $[0, 50]$ evolving over time $t \in [0, 10000]$. In the upper heatmap, a wavelike starfish front moves from 0 to $L = 50$. However, in contrast to a traveling wave as defined in chapter (3), the starfish front is slowing down during its progress. At first glance, the starfish wavefront position seems to follow a power law $\approx t^{\frac{1}{2}}$.
Second, it is noticeable that there is continuously a small amount of starfish left behind, as the front propagates. At time $t = 10000$, the starfish have diffused and reached a constant density in the whole space. This is consistent with $D_k(M) > 0$ for all $k > 0$ and $M \leqslant 0$, which means that the starfish are able to diffuse over any bounded distance, given enough time. The lower heatmap visualises the development of the mussel bed. It shows a sharp boundary between the untouched and the harvested area. The simulation suggests that the starfish front and this boundary are at the same position x at each time t. Thus, mussel harvesting also seems to follow a power law $\approx t^{\frac{1}{2}}$.
From a biological point of view, it is of great interest to know at which speed the starfish front propagates. For fishers and biologists, it is important to know how fast starfish can invade and erase huge mussel bed regions. Besides, it is actually possible to measure the progression speed of a starfish front (cf. Dare (1982)) and thus to verify, calibrate and adapt the model and its parameters.
First, it is necessary to define the position of the wavefront with robust statistics, to overcome possible inaccuracies due to the simulation's resolution. There are two possible approaches to define the wavefront position, either from the starfish progression or from the mussel harvesting point of view:

1. Starfish wavefront: From the starfish point of view, the wavefront is at position x,

where the starfish population has a peak (=maximum). However, this might not be a reliable and robust measure (cf. figure (13)), because the peaks are not sharp enough in the numerical resolution provided.

2. Mussel wavefront: From the mussel point of view, the wavefront is at position x, where half of the mussels have been erased. Figure (14) suggests that this point can be determined in a sufficiently precise way.

Figures (13) and (14) show the starfish wavefront progression and the mussel wavefront progression on the interval $[0, 50]$. From approximately $6 \cdot 10^5$ starfish waves computed by ode45, every 5000th is plotted and from $6 \cdot 10^5$ mussel waves, every 10000th is plotted. Diffusion causes the starfish wave to reach a uniformly distributed density of $0.02 = \frac{1}{50}$ in the end.

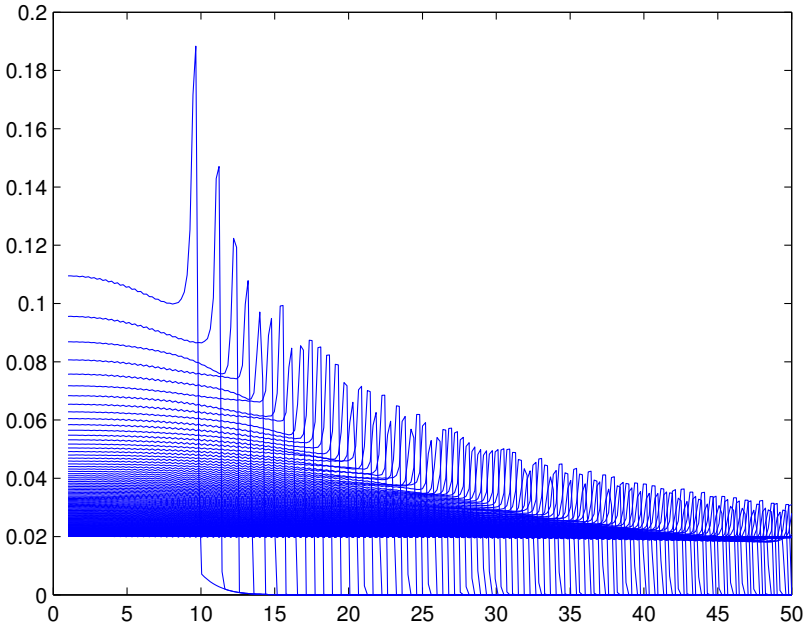

Figure 13: Starfish density wavefront progression on the interval $[0, 50]$

Obviously, the mussel wavefront forms a much clearer boundary than the starfish peak. This suggests, that from a numerical point of view, it is more feasible to use the mussel data as definition for the wavefront's position. The following sections compare the two approaches.

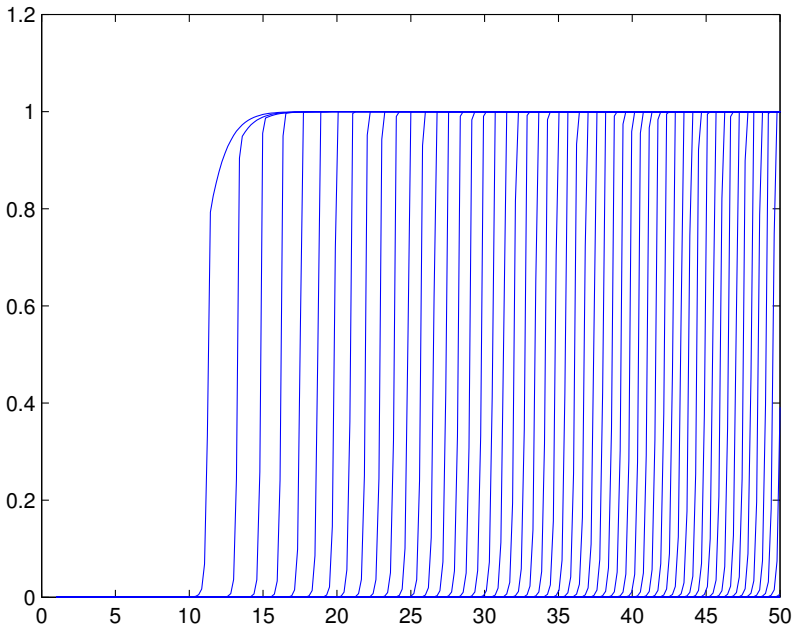

Figure 14: Mussel density wavefront progression on the interval $[0, 50]$

6.1 Wavefront speed and amplitude

6.1.1 Starfish wave amplitude

Figure (13) suggests that the starfish peak follows a power law:

$$\max_{x\in[0,50]} S(x,t) \approx t^{-1} \tag{44}$$

Indeed, figure (15) showing the progression of the starfish wave on [0,50] in comparison to t^{-1}, confirms this hypothesis. For the plot, every 500th wave of the $6 \cdot 10^5$ computed by ode45 was selected.

6.1.2 Starfish wavefront speed

From a statistical point of view, it is not recommendable to use the maximum starfish density to mark the position of the starfish front, since the maximum is not a robust statistic and might thus be affected by numerical inaccuracies. Figure (13) illustrating the starfish wavefront at different time points suggests that the left behind starfish form a tail, which becomes less and less dense over time. Thus, it is plausible to use the spatial starfish spread as a measure for the front's progression. One possible measure for the

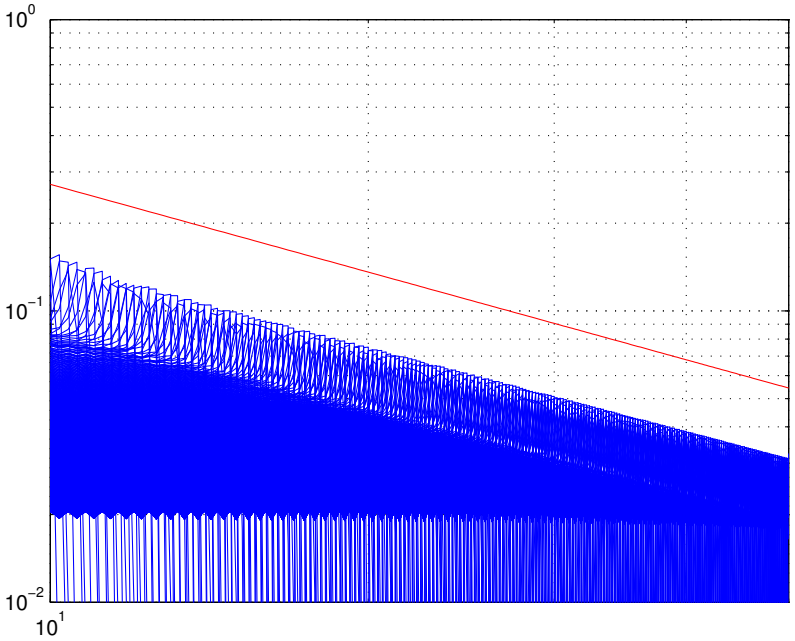

Figure 15: Starfish density wavefront progression (blue) on the interval [10,50] compared to t^{-1} (red) in a loglog-plot

spatial starfish spread is entropy, which is defined for a pdf (probability density function) $f(x)$ as follows:

Definition 3. *Entropy:* $E_f \coloneqq -\int_{-\infty}^{\infty} f(x)\ln(f(x))\,dx$

The entropy corresponds to $-\mathbb{E}\log(X)$, when X is a sample from a probability distribution $f(x)$. Since the advection-diffusion equation conserves mass, the starfish distribution $S(x,t)$ is a pdf for every fixed point in time t. Thus, we can compute

$$E_S(t) = -\int_{-\infty}^{\infty} S(x,t)\ln(S(x,t))\,dx \tag{45}$$

Figure (16) shows the exponential starfish entropy $\exp(E_S(t))$ (magenta) over time. It is monotonously increasing and reaches a level of 50 at the end of the time span. This corresponds to the length of the interval $[0,50]$ and is due to the fact that a uniformly distributed random variable on an interval $[0,L]$ has entropy $\ln(L)$. Hence, diffusion causes the starfish to spread uniformly on the whole space after all the mussels are harvested. The increasing number of starfish left behind in the tail (cf. figure 13) are no longer part of the wavefront peak and cause the entropy to rise over time. The asymptotic

behaviour of starfish entropy is compared to a power law of $\approx t^{\frac{1}{2}}$ (blue). This means that in the final phase of the simulation, starfish entropy grows with the square root of time, before it reaches the final level 50, the upper boundary to starfish entropy.

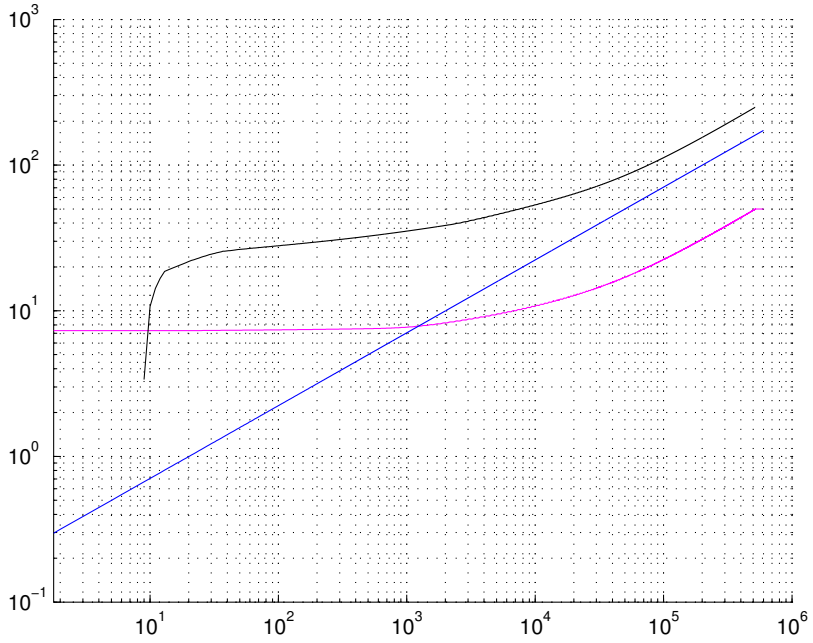

Figure 16: Exponential starfish entropy (magenta) and mussel wavefront position (black) compared to $t^{\frac{1}{2}}$ (blue) over time

6.1.3 Mussel wavefront speed

Plotting the mussel waves over time, it is evident that they show a much steeper wavefront than the starfish waves (cf. figure (14)). Thus, the position of the wavefront from the mussel point of view is defined as the position x, where $M(x,t)$ is closest to $\frac{1}{2}$.
To reach a higher resolution, interpolation was used. At any instant of time t, Matlab's function interp1 was used to find the real number $x \in [0, 50]$, where the interpolated discretized function $M(x,t)$ is closest to 0.5. These positions were plotted in figure (16) (black). Note that the data from the beginning and the end of the simulation was omitted, because then the mussel wavefront is not yet formed or already erased. Just as starfish entropy, the mussel wavefront position is monotonously increasing over time and asymptotically growing $\approx t^{\frac{1}{2}}$.

6.1.4 Comparison starfish and mussel wavefront

Thus, both approaches to define the wavefront positions yield the same conclusion. The asymptotical growth of $\exp(E_S(t))$ and the mussel wavefront position follow a $t^{\frac{1}{2}}$ power law. This means that either of those approaches can be used to define the wavefront position, which suggests using the mussel wavefront since it is clearer to depict the position where $M(x,t) = 0.5$ than starfish entropy.

6.2 Scaling-invariant system

Figures (13) and (14) give reason to the hypothesis that the system's underlying dynamics might be scaling-invariant. This subsection will collect various evidence for this hypothesis.

6.2.1 Starfish wavefront

Figure (13) suggests that the starfish density $S(x,t)$ might be a function σ of the wavefront position $\exp(E_S(t))$ in terms of the exponential starfish entropy (cf. section (6.1.2)).

$$S(x,t) = \sigma\left(\frac{x}{\exp(E_S(t))}\right)\frac{1}{\exp(E_S(t))} \tag{46}$$

Figure (17) shows the scaled starfish wavefronts on $[0,6] \subset [0,50]$. It was decided to choose one wavefront rather from the beginning, one wavefront from the middle and one wavefront rather from the end of the simulation to test the hypothesis on the wavefront shapes at different times in the simulation. From $6 \cdot 10^5$ waves the 10^5th, $2 \cdot 10^5$th and the $5 \cdot 10^5$th were selected, scaled by the exponential starfish entropy

$$S(x,t)\exp(E_S(t)) \tag{47}$$

and plotted over a scaled x-axis, which was multiplied by $\frac{1}{E_S(t)}$. The result supports the hypothesis, because the scaled curves overlap quite well.
Since the mussel wavefront was clearer to determine by the position x, where $M(x,t) \approx 0.5$, it suggests scaling with the mussel wave. Figure (18) shows the same as figure (17) with the starfish curves scaled by $M_{0.5}(t)$:

$$S(x,t) = \sigma\left(\frac{x}{M_{0.5}(t)}\right)\frac{1}{M_{0.5}(t)} \tag{48}$$

Both figure (17) and (18) are quite promising and give similar results. This means that

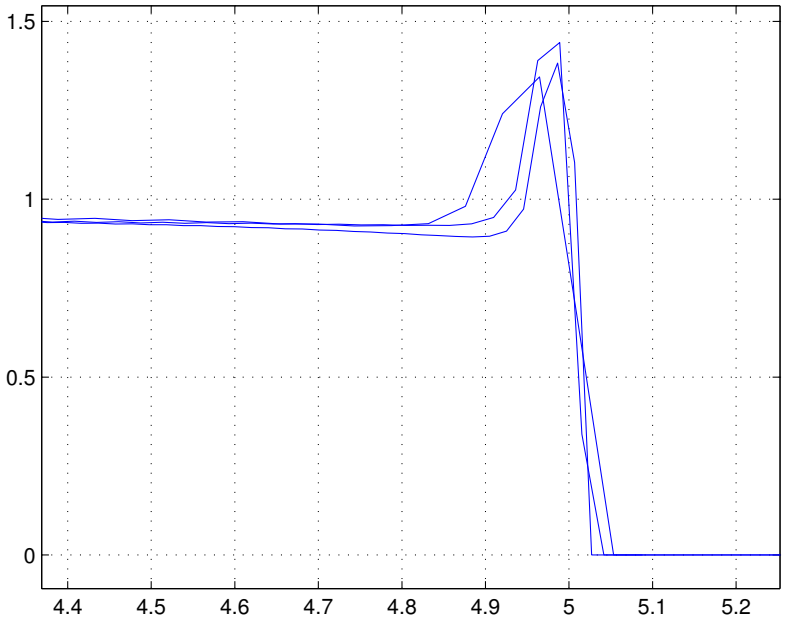

Figure 17: Starfish wavefront scaled with exponential entropy $\exp(E_S(t))$ over x-axis scaled with $\frac{1}{E_S(t)}$

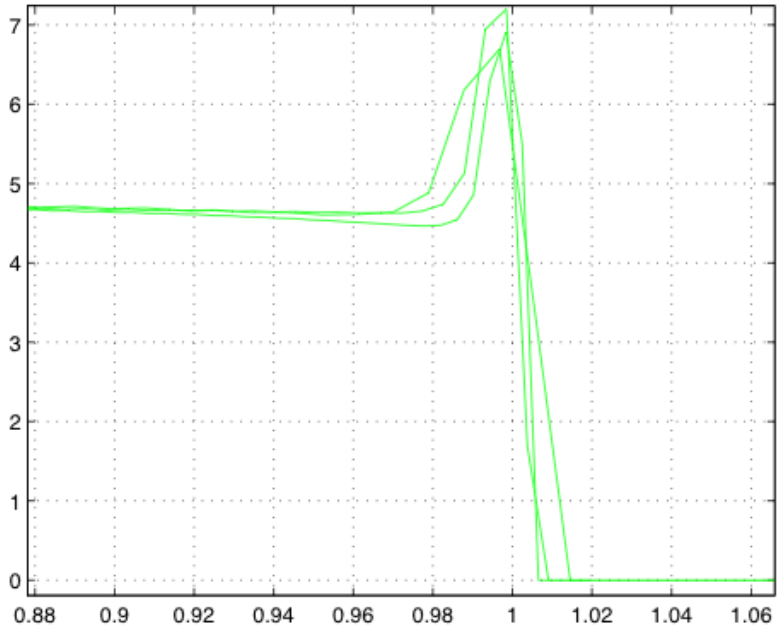

Figure 18: Starfish wavefront scaled with the position of mussel half $M_{0.5}(t)$ over x-axis scaled with $\frac{1}{M_{0.5}(t)}$

both scaling variants can be useful and give reason to the hypothesis that the starfish wavefront may be a scaling-invariant phenomenon.

6.2.2 Mussel wavefront

The mussel wavefront allowed a direct definition of the wavefront in terms of the position x, where the mussel density is 0.5. Figure (14) gives reason to the hypothesis that the mussel wavefront shifts over time, but needs not be scaled since all waves have the same amplitude.
Figure (19) shows the shifted mussel waves. The first 10^5 waves were omitted to capture the system's dynamic without the initial condition's influence. Then, every 500th wave was shifted, so that $M(0,t) = \frac{1}{2}$ at all times t. The result is quite convincing for the grazing process between $0 < M(x,t) < 0.75$, however the grazing process between $0.75 < M(x,t) < 1$ does not seem to be captured in a satisfying manner.
Thus, in figure (20) the mussel waves are not only shifted, but also scaled. The scaling process was done as follows:
By means of interpolation the positions $M_{75}(t), M_{50}(t)$ and $M_{25}(t)$ were computed as the x-values, where $M(x,t) = 0.75, 0.5, 0.25$. Then the difference Δ was computed for all times t

$$\Delta(t) \coloneqq M_{0.75}(t) - M_{0.25}(t) \tag{49}$$

as well as the scaled x-value x_{new}, where x_{old} denotes the unscaled x-axis:

$$x_{\text{new}}(t) \coloneqq \frac{x_{\text{old}}(t) - M_{0.5}(t)}{\frac{\Delta(t)}{2}} \tag{50}$$

However, the scaled and shifted waves do not only fail at improving the issue in the interval $0.75 < M(x,t) < 1$, but also fail at capturing the mussel harvesting between $0 < M(x,t) < 0.3$. This leads to the conclusion that the mussel wavefront is not invariant to scaling in form of the upper ansatz.

6.3 Conclusion

The simulations yielded that the starfish show a wavelike behaviour, but do not form a traveling wave in the classical sense. There are continuously some starfish left behind and the maximum starfish peak is decreasing over time. At the same time the wave progression speed is slowing down. The hypothesis that the mussel wavefront might

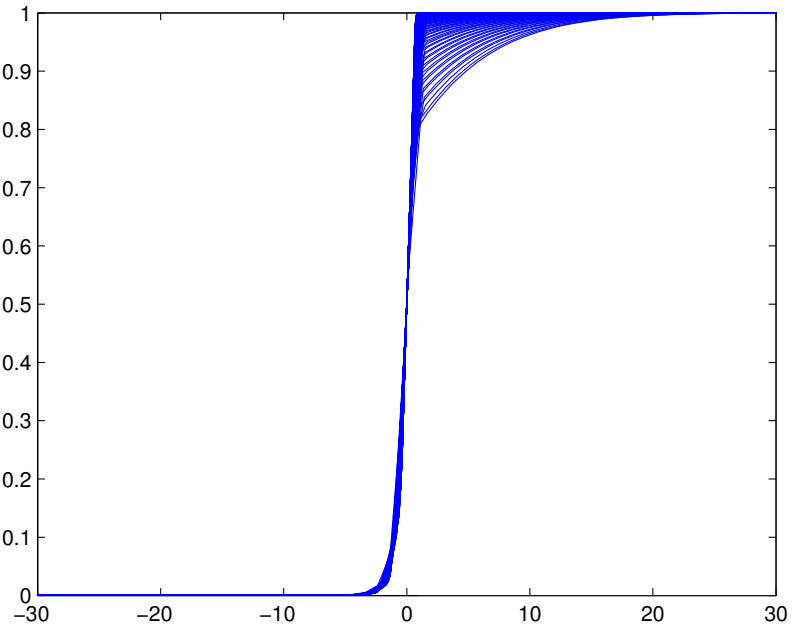

Figure 19: Mussel wavefront shifted

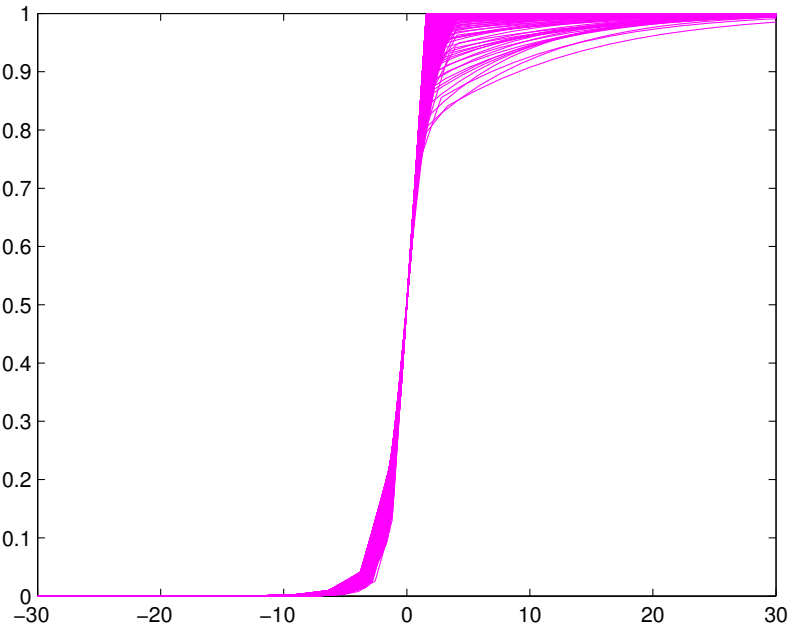

Figure 20: Mussel wavefront shifted and scaled

be scaling-invariant was not confirmed by the results in this chapter. However, the starfish wavefront probably underlies some scaling-invariant phenomenon, which will is an interesting result and worth being investigated in future works.

7 Analytical results on the advection-diffusion model without mussel growth

7.1 Equilibrium points of the PDE system

First, the equilibrium points will be determined. For this model the equilibrium points are $(\bar{S}, \overline{M})$ with $\bar{S}$ and $\overline{M}$ being nonnegative functions on $[0, 50]$ describing the initial and permanent mussel and starfish distribution. An equilibrium requires $\dot{S} = 0$ as well as $\dot{M} = 0$. This means, the mussel and starfish densities are constant in time. Using $\dot{M} = 0$, equation (25) yields the condition:

$$0 = -h(M)S \tag{51}$$

This implies $S \equiv 0$, since $h(M(x)) > 0$ for all $M(x) > 0$. Thus, the points $(0, \overline{M})$ with $\overline{M}$ being any nonnegative function in x on $[0, 50]$ are equilibria. Besides, all points $(\bar{S}, 0)$ with $\bar{S} = \text{const}$ are equilibria, because then all derivatives of S are 0. Further, $M \equiv 0$ implies $\frac{\partial^2 D(M)}{\partial x^2} = 0$ and thus the following equation holds for all constant functions S:

$$\begin{aligned} 0 = \dot{S} =& (DS)'' && (52)\\ =& (D'S + DS')' && (53)\\ =& D''S \underbrace{+ D'S' + D'S' + DS''}_{=0} && (54)\\ =& D''S && (55) \end{aligned}$$

The equilibrium points $(0, \overline{M})$ with $M(x, t) = M(x)$ being a nonnegative function describe the scenario, with an arbitrary mussel bed without starfish harvesting it. Since the model includes neither a mussel growth nor death process, there is no change over time.

The equilibrium points $(\bar{S}, 0)$ with $S(x, t) = \text{const}$ correspond to the situation, that there are no mussels present. Further, the starfish are uniformly spread and thus not subject to diffusion.

These are the only equilibrium points. As soon as the starfish population is not uniformly spread or in case that both mussels and starfish are present, the system will change over time, since either the starfish will diffuse or harvest the mussel bed.

7.2 Absence of traveling waves

In this section, it will be proved that the PDE system has no traveling wave solutions in the classical sense (cf. chapter (3)) with the property $\lim_{z\to\infty} S(z) = 0$. With a traveling wave ansatz $z = x - ct$, the coupled PDE system can be transformed into an ODE system.
For the mussel density $M(x,t) = M(x-ct) = M(z)$ the chain rule is used:

$$\frac{\partial M}{\partial t} = -c\frac{dM}{dz}\frac{\partial z}{\partial t} = -c\frac{dM}{dz} \tag{56}$$

This yields the new equation:

$$\frac{dM}{dz} = \frac{1}{c}h(M(z))S(z) \tag{57}$$

For the starfish density $S(x,t) = S(x-ct) = S(z)$ follows in analogy:

$$-c\frac{dS}{dz} = \frac{d^2}{dz^2}\left[D(M(z))S(z)\right] \tag{58}$$

Thus, the traveling wave ansatz yields the following coupled ODE system:

$$-c\frac{dS}{dz} = \frac{d^2}{dz^2}\left[D(M(z))S(z)\right] \tag{59}$$

$$\frac{dM}{dz} = \frac{1}{c}h(M(z))S(z) \tag{60}$$

Proposition. *The ODE system defined by equations (59) and (60) with* $h(M) = \frac{\alpha M}{M+k_M}$ *has no traveling wave solutions in the classical sense with the property* $\lim_{z\to\infty} S(z) = 0$.[6]

Proof. Equation (59) yields:

$$-c\frac{dS}{dz} = \frac{d^2}{dz^2}\left[D(M(z))S(z)\right] \tag{61}$$

$$-cS' = (DS)'' \tag{62}$$

$$(DS)'' + cS' = 0 \tag{63}$$

$$[(DS)' + cS]' = 0 \tag{64}$$

$$(DS)' + cS = \text{const} \tag{65}$$

[6] This means that in front of the wave there are no starfish, which is a reasonable assumption from a biological point of view. We are interested in describing invasion waves entering a new territory. Thus, there are no starfish present before the wave arrives.

Under the assumption that in the limit $z \to \infty$ there are no starfish present, this constant must be 0.

Thus, equation (60) and (65) yield the coupled ODE system:

$$\frac{dD}{dM}\frac{dM}{dz}S + D\frac{dS}{dz} + cS = 0 \tag{66}$$

$$c\frac{dM}{dz} = h(M)S \tag{67}$$

Substituting $\frac{dM}{dz} = \frac{h(M)}{c}S$, this ODE system can be rewritten as follows, note the wave speed $c > 0$ and the diffusivity function $D(M) > 0$ for all M:

$$S' = -\frac{c}{D(M)}S - \frac{D'(M)h(M)}{D(M)c}S^2 \tag{68}$$

$$M' = \frac{h(M)}{c}S \tag{69}$$

Now, the steady states with $S' = M' = 0$ will be determined. Obviously, all points $(S, M) = (0, M)$ fulfill this. In this case, the mussel beds rest untouched, because there are no starfish. These are the only points, because $M' = 0 \Rightarrow S = 0$, since the harvesting function $h(M)$ is strictly positive for all $M > 0$:

Consider now the equation:

$$\frac{S'}{M'} = -\frac{c^2}{D(M)h(M)} - \frac{D'(M)}{D(M)}S \tag{70}$$

This yields the following trajectories in the phase plane:

$$\frac{dS}{dM} = -\frac{c^2}{D(M)h(M)} - \frac{D'(M)}{D(M)}S \tag{71}$$

This is a linear ODE in $S(M)$, which gives closed solutions. Rearranging the system yields:

$$D(M)\frac{dS}{dM} = -D'(M)S - \frac{c^2}{h(M)} \tag{72}$$

The chain rule yields:

$$\frac{d(DS)}{dM} = D(M)\frac{dS}{dM} + S\frac{dD(M)}{dM} \tag{73}$$

Inserting equation (72) into equation (73) yields:

$$\frac{d(DS)}{dM} = -\frac{dD(M)}{dM}S - \frac{c^2}{h(M)} + S\frac{dD(M)}{dM} \tag{74}$$

$$= -\frac{c^2}{h(M)} \tag{75}$$

The fundamental theorem of calculus implies for an $\epsilon > 0$:

$$D(M)S = -c^2 \int_\epsilon^M \frac{1}{h(n)} dn \tag{76}$$

This yields the following representation of $S(M)$:

$$S(M) = -\frac{c^2}{D(M)} \int_\epsilon^M \frac{1}{h(n)} dn \tag{77}$$

To compare the results to the situation in the numerical simulation, from now on $h(M) = \frac{\alpha M}{M+k_M}$:

$$D(M)S = -c^2 \int_\epsilon^M \frac{n + k_M}{\alpha n}\, dn \tag{78}$$

$$= -c^2 \int_\epsilon^M \left[\frac{1}{\alpha} + \frac{k_M}{\alpha}\frac{1}{n}\right] dn \tag{79}$$

$$= -c^2 \left[\frac{n}{\alpha} + \frac{k_M}{\alpha}\ln(n)\right]\Bigg|_\epsilon^M \tag{80}$$

$$= -\frac{c^2}{\alpha}\left[M + k_M \ln(M) - \epsilon - k_M \ln(\epsilon)\right] \tag{81}$$

This results in the following representation of $S(M)$:

$$S(M) = -\frac{c^2}{\alpha D(M)}\left[M + k_M \ln(M) - \epsilon - k_M \ln(\epsilon)\right] \tag{82}$$

$$= \underbrace{-\frac{c^2}{\alpha D(M)}}_{<0 \text{ and bounded}} \left[M + k_M \ln\left(\frac{M}{\epsilon}\right) - \epsilon\right] \tag{83}$$

Consider now the limit $M \to 0$:

$$\lim_{M\to 0} S(M) = \lim_{M\to 0} \underbrace{-\frac{c^2}{\alpha D(M)}}_{<0 \text{ and bounded}} \left[M + k_M \ln\left(\frac{M}{\epsilon}\right) - \epsilon \right] = \infty \tag{84}$$

since $\lim_{M\to 0} \ln\left(\frac{M}{\epsilon}\right) = \infty$ for all $\epsilon > 0$.

□

7.3 Comparison to the numerical results

This means, that under the assumption of a front invading a former uninhabited territory the model with harvesting function $h(M) = \frac{\alpha M}{M+k_M}$ does not allow traveling wave solutions. This result might come as a surprise, since in chapter (3) it was stated that advection-diffusion equations have traveling wave solutions. However, the result corresponds to the numerical simulation in chapter (5), which produced wavelike phenomena, but not traveling waves in a classical sense. That leads immediately to the question, which of these restrictions can be lowered to actually obtain traveling wave solutions. Further, it would be of interest to investigate the situation for different harvesting functions, which might be an interesting approach in future works. Another possibility is to include mussel growth into the model and study the effects on the system's stability. This will be done in the subsequent chapter (8), where a criterion how mussel growth affects the system's stability, will be derived.

8 Stability in the spatial & the non-spatial model with mussel growth

8.1 Spatial model including mussel growth

Up to now, mussel growth has been neglected, since it is considered to be much slower than the starfish movement. However, it is of interest, if the system's stability will change, when mussel growth is taken into consideration. This chapter investigates the consequences, if the mussel population is not only subject to starfish harvesting, but also to other changes such as growth or natural death. This yields a more complex model, where $f(M)$ denotes changes in the mussel population:

$$\begin{aligned} \frac{\partial S}{\partial t} &= \frac{\partial^2 (DS)}{\partial x^2} \\ \frac{\partial M}{\partial t} &= -h(M)S + f(M) \end{aligned} \tag{85}$$

A natural choice for the function $f(M)$ could be for instance a logistic growth function, e.g. $f(M) = M(1 - M)$. However, the approach in this chapter will be general and without further specification of $f(M)$.

8.2 Non-spatial model including mussel growth

For reasons of comparison, the non-spatial version of the upper model will also be mentioned. This simple model describes the starfish predating on mussels without spatial dynamics in terms of diffusion. Again, the mussel population is subject to changes described by the function $f(M)$:

$$\begin{aligned} \dot{S} = S' &= 0 \\ \dot{M} &= -h(M)S + f(M) \end{aligned} \tag{86}$$

From the first equation follows $S(x,t) = \bar{S}$ with $\bar{S} = \text{const} \in \overline{\mathbb{R}^+}$ for all $x \in \overline{\mathbb{R}^+}$ and $t \in \overline{\mathbb{R}^+}$.

8.3 Stability analysis for the spatial model with mussel growth

The following section comprises a stability analysis of the linearized version of the spatial model including growth, governed by the PDE system (85). The central part is to show

that the following proposition holds:

Proposition. *Stability in the non-spatial system implies stability in the spatial system. Neither the wave number m, nor the diffusivity function $D(M)$ change the system's stability. However, an unstable non-spatial system might become stable by choosing a suitable diffusivity function.*

8.3.1 Equilibrium points

Evidently, the system has the same equilibrium points as the non-spatial model (86). Additionally, there are equilibrium points, when $D''(\overline{M}) = 0$, for $\overline{M}$ implicitly defined by the equation $h(\overline{M})\bar{S} = f(\overline{M})$, where $\bar{S}$ is an arbitrary positive value.

8.3.2 Stability analysis

In this paragraph, a stability analysis for the equilibrium points, where $\bar{S} \neq 0$, will be conducted.
The following ansatz is used, where ϵ denotes a small positive number and $\widetilde{S}$ respectively $\widetilde{M}$ disturbances of the starfish and mussel equilibrium points:

$$S(x,t) = \bar{S} + \epsilon\widetilde{S}(x,t) \tag{87}$$
$$M(x,t) = \overline{M} + \epsilon\widetilde{M}(x,t) \tag{88}$$

Inserting this ansatz into the equation system (86) yields:

$$\epsilon\frac{\partial\widetilde{S}}{\partial t} = \left(D(\overline{M} + \epsilon\widetilde{M}(x,t))(\bar{S} + \epsilon\widetilde{S})\right)'' \tag{89}$$
$$\epsilon\frac{\partial\widetilde{M}}{\partial t} = -h(\overline{M} + \epsilon\widetilde{M}(x,t))(\bar{S} + \epsilon\widetilde{S}) + f(\overline{M} + \epsilon\widetilde{M}(x,t))) \tag{90}$$

A Taylor series approach is used to linearize the functions $D(\overline{M} + \epsilon\widetilde{M}(x,t))$, $h(\overline{M} + \epsilon\widetilde{M}(x,t))$ and $f(\overline{M} + \epsilon\widetilde{M}(x,t)))$. This yields the following linearized system:

$$\epsilon\frac{\partial\widetilde{S}}{\partial t} = \left(\left(D(\overline{M}) + \epsilon\widetilde{M}(x,t)\frac{\partial D}{\partial M}\bigg|_{M=\overline{M}}\right)\left(\bar{S} + \epsilon\widetilde{S}\right)\right)'' \tag{91}$$
$$\epsilon\frac{\partial\widetilde{M}}{\partial t} = -\left[h(\overline{M}) + \epsilon\widetilde{M}(x,t)h'(\overline{M})\right]\left(\bar{S} + \epsilon\widetilde{S}\right) + f(\overline{M}) + \epsilon\widetilde{M}(x,t)f'(\overline{M}) \tag{92}$$

Rearranging after powers of ϵ yields for the starfish equation:

$$\epsilon \frac{\partial \widetilde{S}}{\partial t} = \left(\left(D(\overline{M}) + \epsilon \widetilde{M}(x,t) \frac{\partial D}{\partial M}\Big|_{M=\overline{M}} \right) \left(\bar{S} + \epsilon \widetilde{S} \right) \right)'' \tag{93}$$

$$= \left(D(\overline{M})\bar{S} \right)'' + \epsilon \left[D'(\overline{M})\widetilde{M}\bar{S} + D(\overline{M})\widetilde{S} \right]'' + \epsilon^2 \left[D'(\overline{M})\widetilde{M}\widetilde{S} \right]'' \tag{94}$$

Division by ϵ yields the following equation for $\frac{\partial \widetilde{S}}{\partial t}$. Further, we use that $0 = \frac{\partial S}{\partial t}|_{S=\bar{S}} = \left(D(\overline{M})\bar{S} \right)''$:

$$\frac{\partial \widetilde{S}}{\partial t} = 0 + \left[D'(\overline{M})\widetilde{M}\bar{S} + D(\overline{M})\widetilde{S} \right]'' + \epsilon \left[D'(\overline{M})\widetilde{M}\widetilde{S} \right]'' \tag{95}$$

Now consider the limit $\epsilon \to 0$:

$$\frac{\partial \widetilde{S}}{\partial t} = \left[D'(\overline{M})\widetilde{M}\bar{S} + D(\overline{M})\widetilde{S} \right]'' + \lim_{\epsilon \to 0} \left(\epsilon \underbrace{\left[D'(\overline{M})\widetilde{M}\widetilde{S} \right]''}_{\text{bounded}} \right) \tag{96}$$

This yields a linear PDE system for $\widetilde{S}$:

$$\frac{\partial \widetilde{S}}{\partial t} = \left[D'(\overline{M})\widetilde{M}\bar{S} + D(\overline{M})\widetilde{S} \right]'' \tag{97}$$

$$= D'(\overline{M})\bar{S}\widetilde{M}'' + D(\overline{M})\widetilde{S}'' \tag{98}$$

In the same way, a linear system for $\widetilde{M}$ can be derived by arranging the terms according to the power of ϵ:

$$\epsilon \frac{\partial \widetilde{M}}{\partial t} = -\left[h(\overline{M}) + \epsilon \widetilde{M}(x,t) h'(\overline{M}) \right] \left(\bar{S} + \epsilon \widetilde{S} \right) + f(\overline{M}) + \epsilon \widetilde{M}(x,t) f'(\overline{M}) \tag{99}$$

$$= \epsilon \left[-h'(\overline{M})\widetilde{M}\bar{S} - \widetilde{S}h(\overline{M}) + f'(\overline{M})\widetilde{M} \right] + \epsilon^2 \left[h'(\overline{M})\widetilde{M}\widetilde{S} \right] \tag{100}$$

Dividing by ϵ and considering the limit $\epsilon \to 0$ yields a linear equation in $\widetilde{M}$:

$$\frac{\partial \widetilde{M}}{\partial t} = -h'(\overline{M})\widetilde{M}\bar{S} - \widetilde{S}h(\overline{M}) + f'(\overline{M})\widetilde{M} \tag{101}$$

In total, a linear PDE system for $\widetilde{M}$ and $\widetilde{S}$ is obtained:

$$\frac{\partial \widetilde{S}}{\partial t} = D'(\overline{M})\bar{S}\widetilde{M}'' + D(\overline{M})\widetilde{S}'' \tag{102}$$

$$\frac{\partial \widetilde{M}}{\partial t} = -h'(\overline{M})\bar{S}\widetilde{M} - h(\overline{M})\widetilde{S} + f'(\overline{M})\widetilde{M} \tag{103}$$

To solve this system, the following ansatz is used. Here $\widehat{S} := S(x = 0, t = 0)$ and $\widehat{M} := M(x = 0, t = 0)$:

$$\widetilde{S}(x,t) = \widehat{S}e^{\lambda t}\cos(mx) \tag{104}$$

$$\widetilde{M}(x,t) = \widehat{M}e^{\lambda t}\cos(mx) \tag{105}$$

Inserting into equations (102) and (103) yields:

$$\lambda\widehat{S}e^{\lambda t}\cos(mx) = \left[D'(\overline{M})\bar{S}\right]\left[-m^2\widehat{M}e^{\lambda t}\cos(mx)\right] + D(\overline{M})\left[-m^2\widehat{S}e^{\lambda t}\cos(mx)\right] \tag{106}$$

$$\lambda\widehat{M}e^{\lambda t}\cos(mx) = \left[-h'(\overline{M})\bar{S} + f'(\overline{M})\right]\left[\widehat{M}e^{\lambda t}\cos(mx)\right] - h'(\overline{M})\widehat{S}e^{\lambda t}\cos(mx) \tag{107}$$

In both equations, the terms $e^{\lambda t}\cos(mx)$ can be cancelled out to get the linear equation system:

$$\lambda\begin{bmatrix}\widehat{S}\\ \widehat{M}\end{bmatrix} = \begin{bmatrix}-m^2D(\overline{M}) & -m^2D'(\overline{M})\bar{S}\\ -h(\overline{M}) & -h'(\overline{M})\bar{S} + f'(\overline{M})\end{bmatrix}\begin{bmatrix}\widehat{S}\\ \widehat{M}\end{bmatrix} \tag{108}$$

To simplify the notation, the following abbreviations are used:

$$a := -m^2D(\overline{M}) \tag{109}$$

$$b := -m^2D'(\overline{M})\bar{S} \tag{110}$$

$$c := -h(\overline{M}) \tag{111}$$

$$d := -h'(\overline{M})\bar{S} + f'(\overline{M}) \tag{112}$$

Definition 4. *A LTI system (linear time-invariant system) is* ***exponentially stable*** *iff all eigenvalues have strictly negative real parts. Exponentially stable systems are also asymptotically stable. In particular, the system will not blow up and oscillations as input will decay exponentially.*

Lemma. *A 2×2-matrix* $A = \begin{bmatrix}a & b\\ c & d\end{bmatrix}$ *is exponentially stable iff both of the following*

criteria hold:

1. $\text{trace}(A) = a + d < 0$

2. $\det(A) = ad - bc > 0$

For biological reasons, the harvesting function $h(M)$ is a monotonic increasing function in M, which means that the derivative $h'(M) \geqslant 0$ for all M. Thus, it holds:

$$c \leqslant 0$$

On the contrary, the diffusivity function $D(M)$ is non-negative and monotonic decreasing, because the fewer mussels, the more the starfish move. This means that $D'(M) \leqslant 0$ for all M. Thus, it also holds:

$$a \leqslant 0$$
$$b \geqslant 0$$

The only matrix entry, which can have either sign is d. Depending on the function $f(M)$, describing the mussel growth process, it might be able to change the sign of the matrix trace as well as the determinant.

From equation (108) two conditions for the system's exponential stability can be obtained. The matrix trace yields the first condition on $f'(\overline{M})$:

$$a + d < 0 \tag{113}$$
$$-m^2 D(\overline{M}) - h'(\overline{M})\bar{S} + f'(\overline{M}) < 0 \tag{114}$$
$$f'(\overline{M}) < \underbrace{m^2 D(\overline{M})}_{>0} + h'(\overline{M})\bar{S} \tag{115}$$

This equation obviously holds for large wave numbers m, for small values of m, the condition might be violated.

The second condition is obtained by the matrix determinant, note that the diffusivity

$D(\overline{M}) > 0$ for all M:

$$ad - bc > 0 \tag{116}$$

$$-m^2 D(\overline{M}) \left[-h'(\overline{M})\bar{S} + f'(\overline{M})\right] - m^2 D'(\overline{M})\bar{S}\, h(\overline{M}) > 0 \tag{117}$$

$$-m^2 D(\overline{M}) \left[-h'(\overline{M})\bar{S} + f'(\overline{M})\right] > m^2 D'(\overline{M})\bar{S}\, h(\overline{M}) \tag{118}$$

$$-h'(\overline{M})\bar{S} + f'(\overline{M}) < -\frac{D'\left(\overline{M}\right)}{D\left(\overline{M}\right)}\bar{S}\, h(\overline{M}) \tag{119}$$

$$f'(\overline{M}) < \underbrace{-\frac{D'\left(\overline{M}\right)}{D\left(\overline{M}\right)}\bar{S}\, h(\overline{M})}_{\geqslant 0} + h'(\overline{M})\bar{S} \tag{120}$$

Thus, two necessary and sufficient conditions for the system's stability have been found:

$$f'(\overline{M}) < \underbrace{m^2 D(\overline{M})}_{>0} + h'(\overline{M})\bar{S} \tag{121}$$

$$f'(\overline{M}) < \underbrace{-\frac{D'\left(\overline{M}\right)}{D\left(\overline{M}\right)}\bar{S}\, h(\overline{M})}_{\geqslant 0} + h'(\overline{M})\bar{S} \tag{122}$$

8.4 Comparison non-spatial & spatial model and conclusion

This section will compare the results of the spatial model to the non-spatial system without diffusion:

$$\dot{S} = S' = 0 \tag{123}$$

$$\dot{M} = f(M) - h(M)\bar{S} \tag{124}$$

This means the equilibrium $\dot{M} = 0$ is equivalent to the equation:

$$f(M) = h(M)\bar{S} \tag{125}$$

Since the system is linear, it is sufficient to consider the Eigenvalues of the Jacobian matrix, which is scalar in this scenario. Thus, the following equation needs to hold for

asymptotical stability:

$$f'(M) - h'(M)\bar{S} < 0 \tag{126}$$

$$f'(M) < h'(M)\bar{S} \tag{127}$$

This condition ensures that equations (121) and (122) hold in any case. It means that in case of a stable non-spatial system, the spatial system will be stable as well. The system's stability can neither be overthrown by the wave number m nor the diffusivity function. Although an unstable non-spatial system might become stable by choosing a suitable diffusivity function. In particular, stability guarantees that the solution will not blow up, i.e. will not approach ∞ in finite time.
Hence, for the advection-diffusion model with mussel growth the choice of the diffusivity function is an important issue and can have significant influence on the system's stability and dynamics.

9 Comparison to other scientists' results

The idea to the model presented in this master thesis was sparked by an article on sea-urchin feeding fronts by Abraham (2007) . He used a Fokker-Planck PDE to model sea-urchins predating on kelp.

9.1 Abraham on sea-urchin feeding fronts

Abraham assumed that each urchin moves in a random walk with a step size only depending on the algae concentration. He used the following advection-diffusion equation to describe the urchin concentration $u(x,t)$ at point x and time t:

$$\frac{\partial u}{\partial t} = \frac{\partial^2}{\partial x^2}(Du) \tag{128}$$

In this model, D describes the urchin motility, which was assumed to be a piecewise constant function depending on an algal density a higher or lower than the threshold a_c:

$$D(a) = \begin{cases} D_- & a < a_c \\ D_+ & a \geqslant a_c \end{cases} \tag{129}$$

Here, $D_- > D_+ > 0$ are constants. Thus, the sea urchins in the model will only move at two different motilities.

9.1.1 Abraham's analytical results

Fixed boundary To obtain an analytical solution for equation (128), Abraham assumed the algal density to be a step function:

$$a(x) \begin{cases} < a_c & x < 0 \\ > a_c & x \geqslant 0 \end{cases} \tag{130}$$

Thus, the starfish motility $D(x,t)$ fulfills at all times t:

$$D(x,t) = \begin{cases} D_- & x < 0 \\ D_+ & x \geqslant 0 \end{cases} \tag{131}$$

Further, it is assumed that the urchins are initially uniformly distributed with a constant $u(x,0) = u_0$ and that the total urchin population is constant. Since the step function

$D(x,t)$ is at no point in time differentiable at $x = 0$, it is a necessary requirement to hold for all t:

$$D_- \lim_{x\to 0^-} u(x,t) = D_+ \lim_{x\to 0^+} u(x,t) \tag{132}$$

To ensure the existence of the derivative $\frac{\partial^2}{\partial x^2}(Du)$ in equation (128), Abraham assumes $\lim_{x\to 0^+} u(x,t)$ and $\lim_{x\to 0^-} u(x,t)$ to be constant in time.[7]
For a constant boundary, the solution to equation (128) can be written in the following way, where $\operatorname{erfc} = 1 - \frac{1}{\sqrt{\pi}} \int_0^x e^{-\beta^2}\, d\beta$ denotes the complementary error function and $\gamma_\pm = \frac{D_+ - D_-}{\sqrt{D_\pm}(\sqrt{D_-}+\sqrt{D_+})}$:

$$u(x,t) = \begin{cases} u_0 \left(1 + \gamma_- \operatorname{erfc}\left(\frac{|x|}{2\sqrt{D_- t}}\right)\right) & x < 0 \\ u_0 \left(1 - \gamma_+ \operatorname{erfc}\left(\frac{|x|}{2\sqrt{D_+ t}}\right)\right) & x \geqslant 0 \end{cases} \tag{133}$$

This function imitates the behaviour of a feeding front with peak at the boundary of the kelp region $x = 0$. Abraham's model produces a predator abundance peak with constant height, but growing width $2\sqrt{D_+ t}$. The starfish wavefront shows a higher density in the kelp region in front of the peak, while behind the front there is a thinned out area.
Figure (21) originates from Abraham (2007) and shows the traveling wave as found by Abraham. In section (9.2) there is a comparison between Abraham's model and the model used in this thesis.

Moving boundary In a second approach, Abraham verified the existence of traveling wave solutions in a system with constant moving boundary at velocity c. He used a traveling wave ansatz $z = x - ct$ to obtain the ODE (cf. chapter (3)), where $u = u(z)$ and $D = D(z)$:

$$-c\frac{du}{dz} = \frac{d^2 Du}{dz^2} \tag{134}$$

The boundary of the kelp region is assumed to be at $z = 0$. The solution to this system is given by the following function, where $u_\infty = \lim_{z\to\pm\infty} u(z)$:

$$\frac{u(z)}{u_\infty} = \begin{cases} 1 & z \leqslant 0 \\ \frac{D_- - D_+}{D_+} e^{\frac{-cz}{D_+}} + 1 & z > 0 \end{cases} \tag{135}$$

[7] This assumption is hardly plausible, but it is necessary for the analytical solution of the equation.

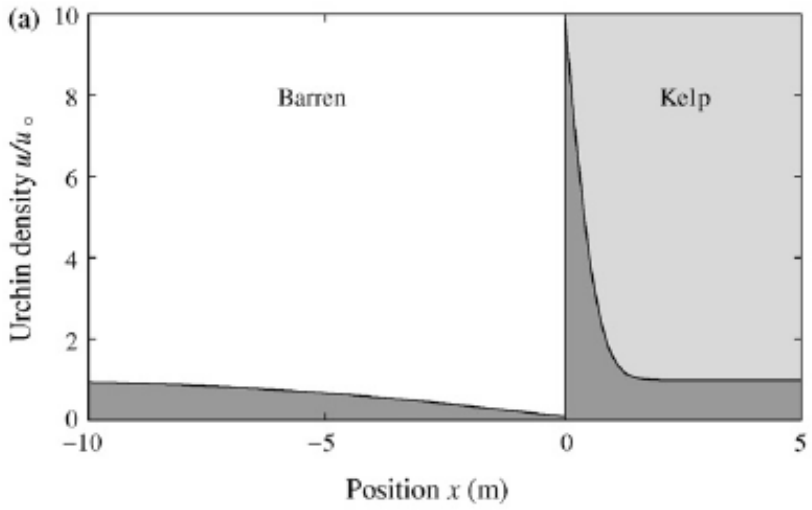

Figure 21: Abraham's traveling wave

Abraham (2007) sums up the results of his model on page 164:

> "[If] $D_- > D_+$, then the traveling wave solution has the form of a feeding front, with a peak at the boundary between the regions. The maximum density within the feeding front occurs on the boundary [...]. The [predator] density is constant throughout the barren region, and decays exponentially towards the ungrazed side of the boundary, the front having a width of $\frac{D_+}{c}$. The feeding front can only propagate continually if there is a non-zero [predator] density within the ungrazed region. Otherwise the front will lose [predators] as it travels and decay away."

9.1.2 Abraham's numerical results

Subsequently, he includes a new equation into the system to allow for seaweed growth $g(s)$ and harvesting $h(s)$ by the urchins u:

$$\frac{\partial s}{\partial t} = g(s) - h(s)u \tag{136}$$

While the growth function $g(s)$ was assumed to be logistic, Abraham chose a Holling type II function as harvesting function $h(s)$:

$$h(s) = \frac{\alpha s}{s + k_s} \tag{137}$$

In this equation, α (dimensions $[su^{-1}t^{-1}]$) denotes the maximal grazing rate per urchin and k_s (dimension [s]) the half-saturation constant for urchin grazing. By numerical simulations, Abraham managed to show that a sea urchin feeding front will be established, which becomes smoother and smoother with time. More details on Abraham's results and a comparison to the results from the model used for this thesis, will be given in the next sections.

9.2 Advection-diffusion model approximating Abraham's model

Abraham used in his model a step function as diffusivity function (cf. section (9.1) and Abraham (2007)). From a biological point of view, this implies that starfish slow down immediately as soon as they reach a certain level of mussel density. Only in areas very scarcely covered by mussels, the starfish move at their usual speed. This approach cannot be implemented directly in the numerical simulation, since the advection-diffusion model needs a differentiable diffusivity function. However, it is possible to approximate a step function on $[0,1]$ with the continuous function series $D_k(M)$, $k \in \mathbb{R}^+$. For the limit $k \to \infty$ the series converges pointwisely:

$$\lim_{k\to\infty} D_k(M) = \lim_{k\to\infty}\left[1 - \frac{1}{1+e^{-kM}}\right] = \begin{cases} 0.5 & M = 0 \\ 0 & M \in (0,1] \end{cases} \tag{138}$$

Proof: For all $k \in \mathbb{R}^+$ holds $D_k(0) = 0.5$.
For every $M \in (0,1]$ holds for all $\epsilon > 0$ that there exists $N(\epsilon, M)$ so that for all $k > N(\epsilon, M)$ holds $D_k(M) < \epsilon$

$$D_k(M) < \epsilon \tag{139}$$

$$1 - \frac{1}{1+e^{-kM}} < \epsilon \tag{140}$$

$$1 - \epsilon < \frac{1}{1+e^{-kM}} \tag{141}$$

$$1 + e^{-kM} < \frac{1}{1-\epsilon} \tag{142}$$

$$e^{-kM} < \frac{1}{1-\epsilon} - 1 \tag{143}$$

$$-kM < \ln\left(\frac{\epsilon}{1-\epsilon}\right) \tag{144}$$

$$k > -\frac{\ln\left(\frac{\epsilon}{1-\epsilon}\right)}{M} =: N(\epsilon, M) \tag{145}$$

Since the limiting function is not continuous on $[0, 1]$, the function series cannot converge uniformly.
For the approximation of Abraham's diffusivity step function in the numerical simulation, the parameter of $D_k(M)$ was set to $k = 50$ and $k = 100$ (cf. figure (22)). From figure (23) and figure (24) it is evident, that the two simulated systems do not show different behaviour any more. This is an indication that the system's dynamic with regard to the limiting function is sufficiently covered in the simulation model. Since the diffusivity is now almost zero for values of $M > 0.1$, it takes the starfish much longer to reach the end of the mussel front at $L = 50$. While in the simulations at the beginning of this chapter, this time period was below 9000, now it is up to 17000. Again, the starfish wave forms a tail of left behind starfish. It is highly remarkable that for these parameter choices the wavefronts actually seem to form traveling waves, while before the wavefront was continually slowing down. This is in line with Abraham's theoretical result that for a step function as diffusivity function traveling waves may emerge (cf. section (9.1)).

9.2.1 Characterising the starfish and mussel wavefront

As already done for the basic model, an analysis will now be carried out on the model for the limiting function. Since the two systems for $k = 50$ and $k = 100$ show similar results, the following analysis will only focus on the case $k = 100$.
Figure (25) compares the positions of the starfish (black) and mussel (magenta) wavefront over time. The mussel wavefront's position was again defined as the position x, where $|M(x, t) - 0.5|$ is smallest. The starfish wavefront's position was measured in terms of $\exp(entropy)$ as defined in section (6.1.2). Once again both definitions show the same asymptotic behaviour. While for the model with $k = 20$ in figure (16) it was a power law of $\approx t^{\frac{1}{2}}$, here it is now $\approx t^{\frac{3}{4}}$ (blue). This means that the diffusivity function has a strong influence on the system's dynamics and the wavefront speed. It suggests that for increasing parameter k the system's dynamics might reach asymptotics of $\approx t$, which would be consistent with a traveling wave. This hypothesis is worth a more profound investigation and is highly recommended for future works to obtain a better understanding of the transition from wavelike phenomena to actual traveling waves when the diffusivity function approaches a step function.

9.2.2 Scaling invariance of the model

Similar to the analysis in chapter (6), it was tested if the model was scaling invariant. However, this time the mussel wavefront position $x_{0.5}(t)$ was not subject to interpolation,

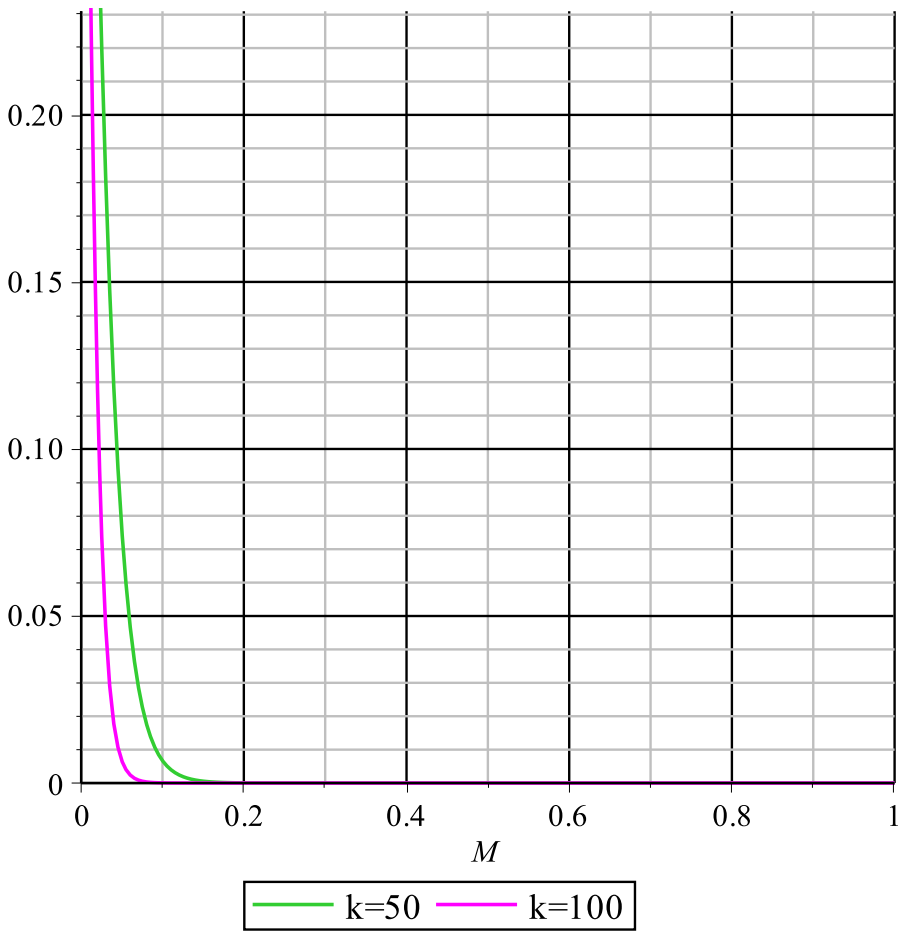

Figure 22: Diffusivity function $D(M) = 1 - \frac{1}{1+e^{-kM}}$ with $k = 50$ and $k = 100$

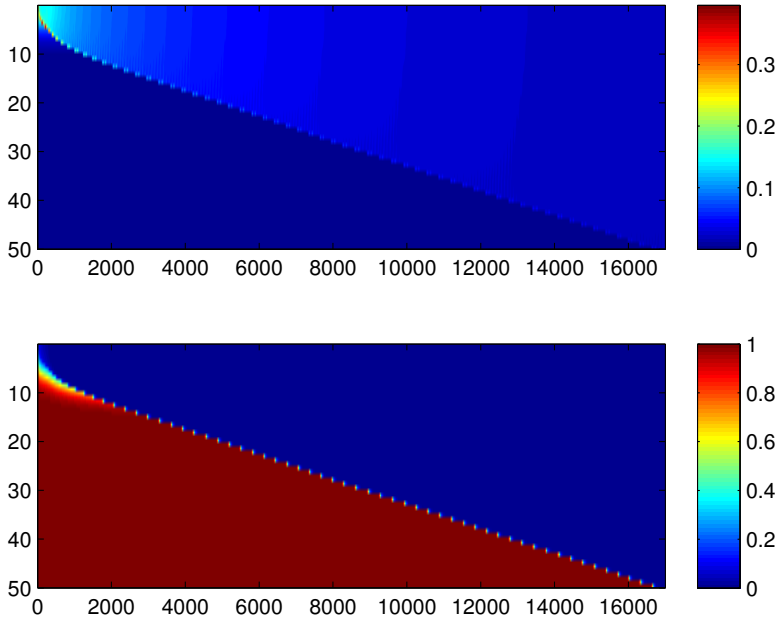

Figure 23: Starfish and mussels with $k = 50$

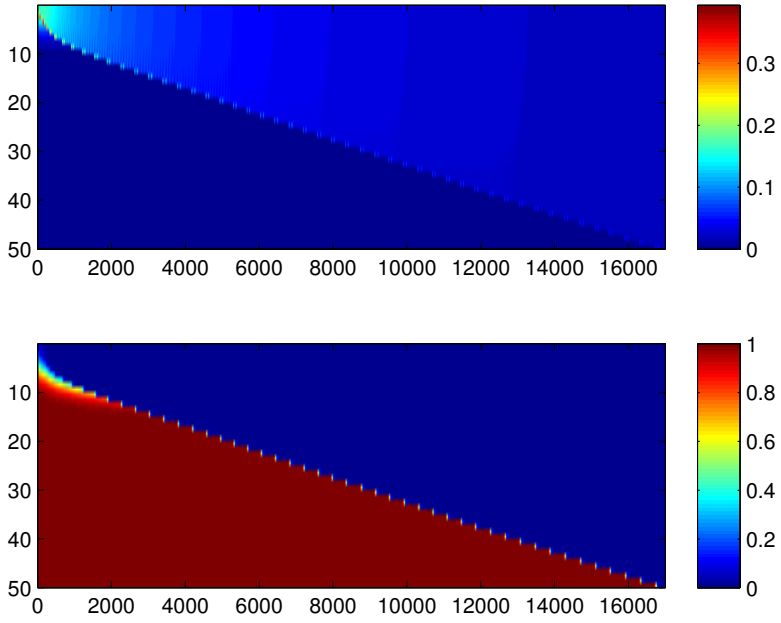

Figure 24: Starfish and mussels with $k = 100$

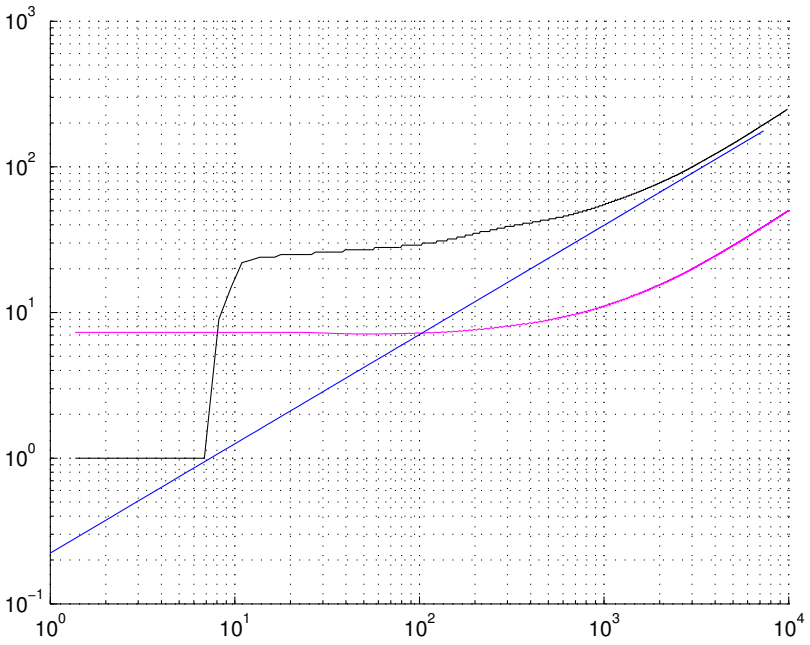

Figure 25: Exponential starfish entropy (pink) and mussel wavefront (black) with diffusivity parameter $k = 100$ on the interval [10,50] compared to $t^{\frac{3}{4}}$ (blue) over time

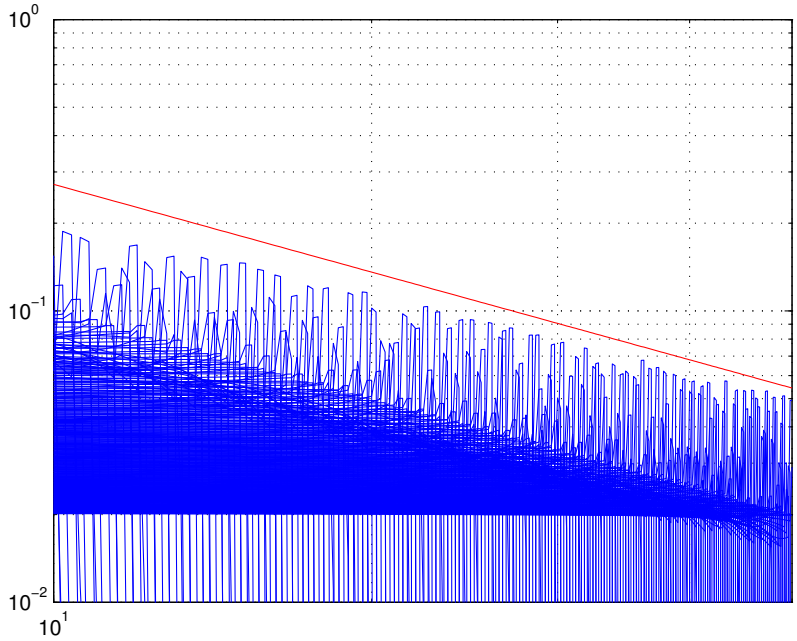

Figure 26: Starfish density wavefront progression $S(x,t)$ (blue) for the diffusivity function parameter $k = 100$ on the interval $[0, 50]$ compared to x^{-1} (red) in a loglog-plot

but directly defined as the position for reasons of simplicity:

$$x_{0.5}(t) = \min_{x\in[0,50],250x\in\mathbb{N}} |M(x,t) - 0.5| \tag{146}$$

The condition $250x \in \mathbb{N}$ ensures that x is a grid point and that the discretized function $M(x,t)$ can be evaluated.

Figure (27) shows every 20^{th} mussel wave shifted by $x_{0.5}(t)$. The last 1000 and the first 1000 waves were omitted to keep the focus on the system's dynamics unaffected by the interval boundaries.

Figure (28) shows the shifted and scaled mussel wavefronts. The following definitions were used to calculated the new x-values:

$$x_{0.25}(t) = \min_{x\in[0,50],250x\in\mathbb{N}} |M(x,t) - 0.25| \tag{147}$$

$$x_{0.75}(t) = \min_{x\in[0,50],250x\in\mathbb{N}} |M(x,t) - 0.75| \tag{148}$$

$$\Delta_{\text{abs}}(t) = x_{0.75}(t) - x_{0.25}(t) \tag{149}$$

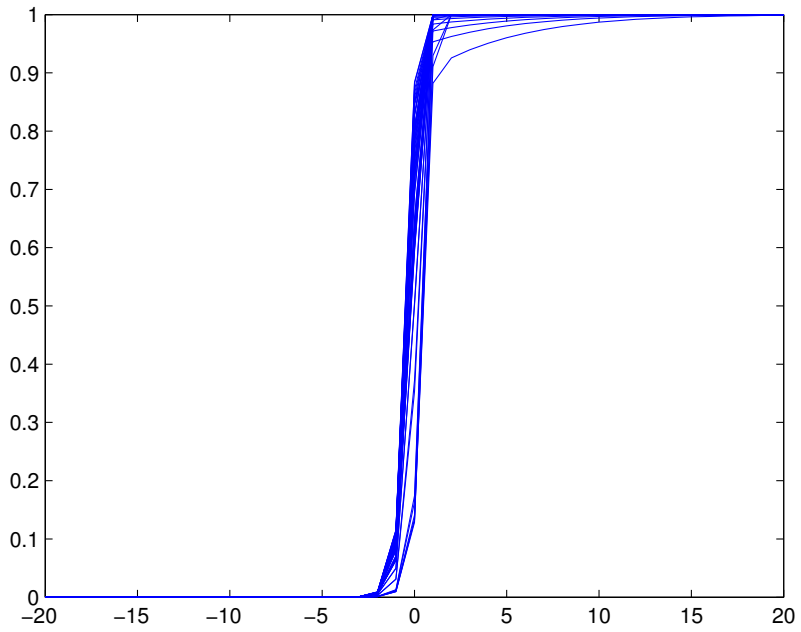

Figure 27: Mussel wavefront for $k = 100$ shifted by $x_{0.5}(t)$

Now, the mussel waves were shifted by $x_{0.5}(t)$ and scaled by $\frac{1}{\frac{\Delta_{\text{abs}}}{2}}$. Again, the last 1000 and the first 1000 were omitted to keep the focus on the system's dynamics unaffected by the interval boundaries.
Although the scaled version gives a fairly satisfying result, the scaled and shifted version shows that the hypothesis of a scaling-invariant system can no longer be supported for the scenario $k = 100$.

9.3 Advection-diffusion model with Abraham's initial condition

In his numerical simulations Abraham chose an initial condition with uniform predator distribution and a linear prey distribution (with small random disturbances). This is exactly the opposing situation to the scenario studied in chapter (5) and corresponds to a theoretical situation, where the predators are uniformly spread on a certain area of the seabed, while the prey aggregation follows a linear function. This scenario might not be plausible from a biological point of view, because predators would rather invade a new area in a wave than be uniformly spread on the whole space. However, it is of interest if these initial conditions imply the same wavelike behaviour, as seen in the preceding simulations.

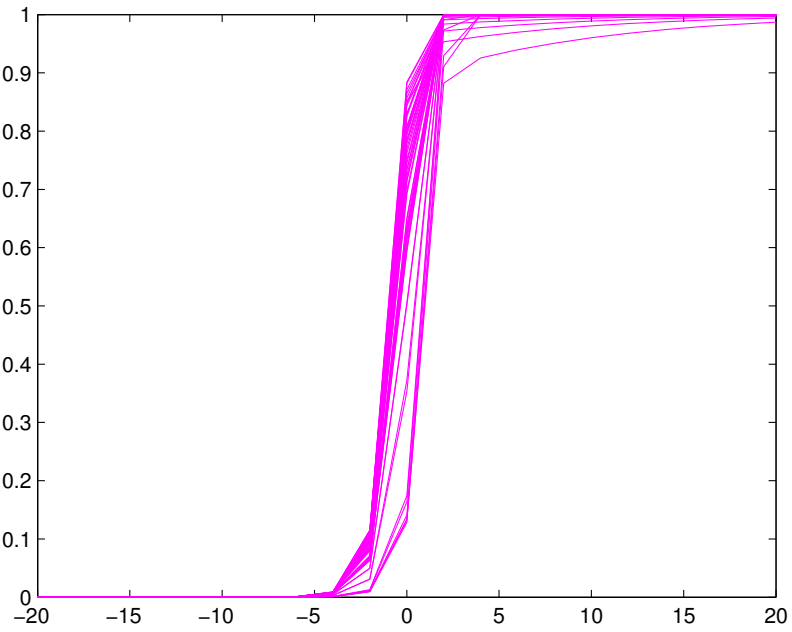

Figure 28: Mussel wavefront for $k = 100$ shifted and scaled

The initial mussel and starfish distribution were set to the following values which correspond to the scenario chosen by Abraham:

$$M(x, 0) = x \tag{150}$$

$$S(x, 0) = \frac{1}{50} \tag{151}$$

All other parameters where chosen like in the basic model in chapter (5), in particular $k = 20$ as parameter for the diffusivity function.
Figure (29) shows a clear and sharp starfish wave traveling from $x = 0$ to $x = 50$ in 19000 time units. This means the starfish wave is able to harvest a mussel bed, where mussel density is a linear function in x, in a traveling wave-like way. In contrast to all the simulations before, this scenario yields a traveling starfish wavefront which seems to have the characteristic properties of a traveling wave:

1. constant amplitude over time
2. constant speed over time
3. constant wave shape over time

This is due to the fact that the diffusivity function lets starfish from regions with very low mussel density move quickly to regions with higher mussel density. While those in regions with higher mussel density stay in their place until the bed at this position is grazed down under specific threshold before they move on.

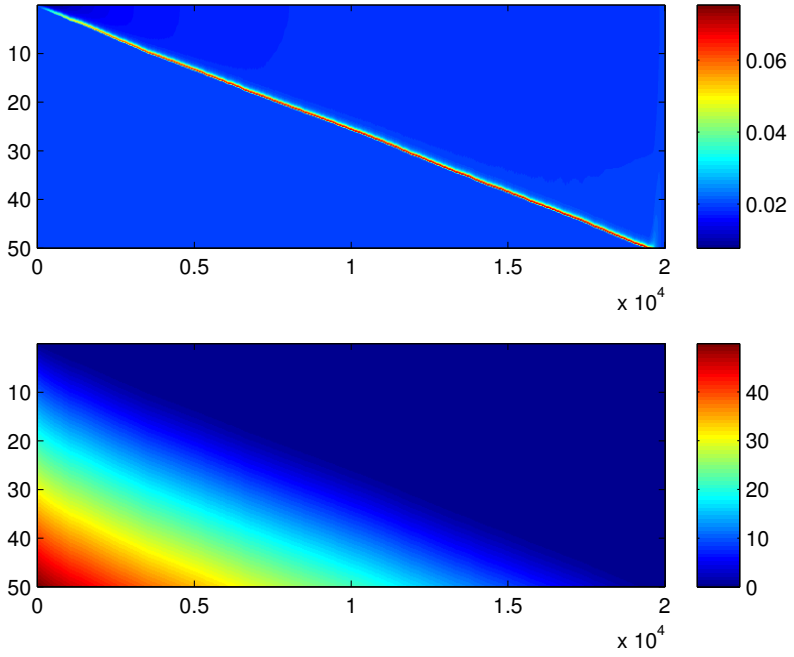

Figure 29: Advection-diffusion model with parameter $k = 20$ and Abraham's initial condition (linear mussel spread, homogenous starfish density)

Figure (30) shows every 50th wave of 2655 computed waves and confirms the hypothesis that the waves formed in this scenario actually are approximately traveling waves. In the end diffusivity causes the starfish again to spread uniformly at a density of $0.02 = \frac{1}{50}$.This is not a contradiction to chapter (7), which includes a proof that no traveling waves can exist for this model. The reason is, that the diffusivity function with $k = 100$ is already almost a step function and might thus approximate a scenario allowing traveling waves. Besides, Abraham's initial condition is a uniformly spread starfish population, which is opposing the assumption of an invasion wave with starfish entering a new and uninhabited territory. From a biological point of view the initial conditions with a linear mussel density and uniform starfish density are not realistic either.
Figure (31) shows a single starfish wavefront at the half time of the simulation and can be compared to Abraham's traveling wave in figure (21). Both waves show a small decay in predator density in the grazed down area behind the wavefront peak. However,

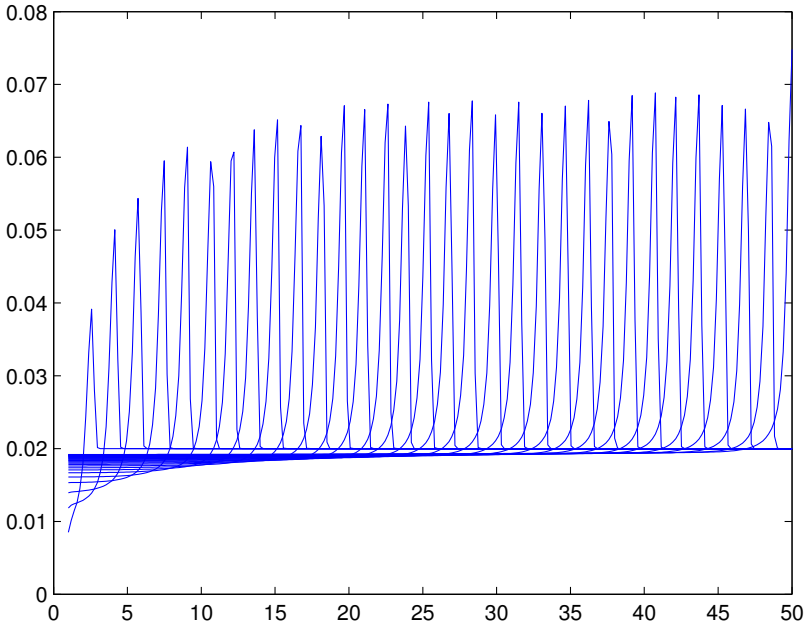

Figure 30: Starfish wavefront progression on the interval $[0, 50]$ in the advection-diffusion model with parameter $k = 20$ and Abraham's initial condition (linear mussel spread, homogenous starfish density)

the transition in front of Abraham's wave is more smooth, while in the scenario in this chapter the wavefront is steep and vice versa for the edge behind the wavefront. A further discussion of this issue can be found in section (9.4).

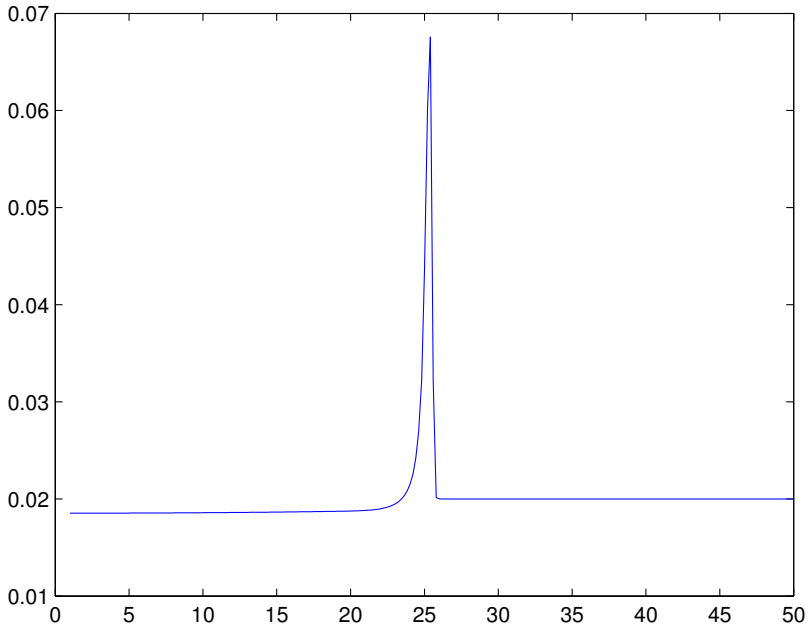

Figure 31: Single starfish wave at simulation half time

9.4 Keller and Segel on bacteria bands

In Keller and Segel (1971a) and Keller and Segel (1971b), the two scientists present their analysis of a model describing bacteria traveling in a tube $[0, L]$ containing an energy source. Their model neglected bacteria growth as well as the substrate's diffusion and focused on the chemotactic response of the bacteria, their diffusive motion and their consumption of the substrate. Thus, this model can be compared to the advection-diffusion model presented in this thesis by identifying starfish with bacteria and mussels with the substrate.

This yields the following PDE model for the substrate concentration $S(x, t)$ and the bacteria concentration $B(x, t)$:

$$\frac{\partial S}{\partial t} = -k(S)b + D\left[\frac{\partial^2 S}{\partial x^2}\right] \tag{152}$$

$$\frac{\partial B}{\partial t} = \frac{\partial}{\partial x}\left[\mu(S)\frac{\partial B}{\partial x}\right] - \frac{\partial}{\partial x}\left[B\chi(S)\frac{\partial S}{\partial x}\right] \tag{153}$$

In these equations, the parameter k denotes the rate of consumption of the substrate per cell and is assumed to be constant, as well as D denoting the substrate's diffusion constant. The function $\mu(S)$ describes the bacteria's motility and is also assumed constant for reasons of simplicity. Finally, the function $\chi(S)$ is the chemotactic coefficient depending on the substrate density.

As initial condition, a constant solution concentration $S_0(x) = S(x, 0)$ is assumed. The boundary conditions correspond to closed ends on both tube sides 0 and L, i.e. no flux through those boundaries:

$$\frac{\partial S(x,t)}{\partial x} = 0 \text{ and } \frac{\partial B(x,t)}{\partial x} = 0 \text{ for } x \in \{0, L\} \tag{154}$$

Keller and Segel state that to obtain traveling wave solutions in their model, it is necessary to have a sufficiently singular chemotactic coefficient $\chi(S)$. Their results show that just as in the advection-diffusion model presented in this master thesis, there is always a certain amount of individuals left behind and not part of the actual wavefront. Of special interest are their investigations concerning the wavefront's shape (cf. figure (32)). The weaker the chemotactic coefficient, the narrower the bacteria band actually is. Further, the band will either be steeper in the front or in the rear, depending on the ratio of the chemotactic coefficient and the bacteria's motility. Lower motility causes the wave to be steeper in the front, a lower chemotactic coefficient yields a wave steeper in the rear.

This suggests that the different wavefront shapes in Abraham's model (cf. figure(21)) and its approximation by the advection-diffusion model (cf. figure (31)) are not necessarily caused by fundamental differences in the modeling approach, but rather by the choice of parameters, i.e. diffusivity and harvesting function.

9.5 Conclusion

Both Abraham (2007) and Keller and Segel (1971b) obtained traveling wave solutions in the classical sense in their advection-diffusion models. However, in both models we

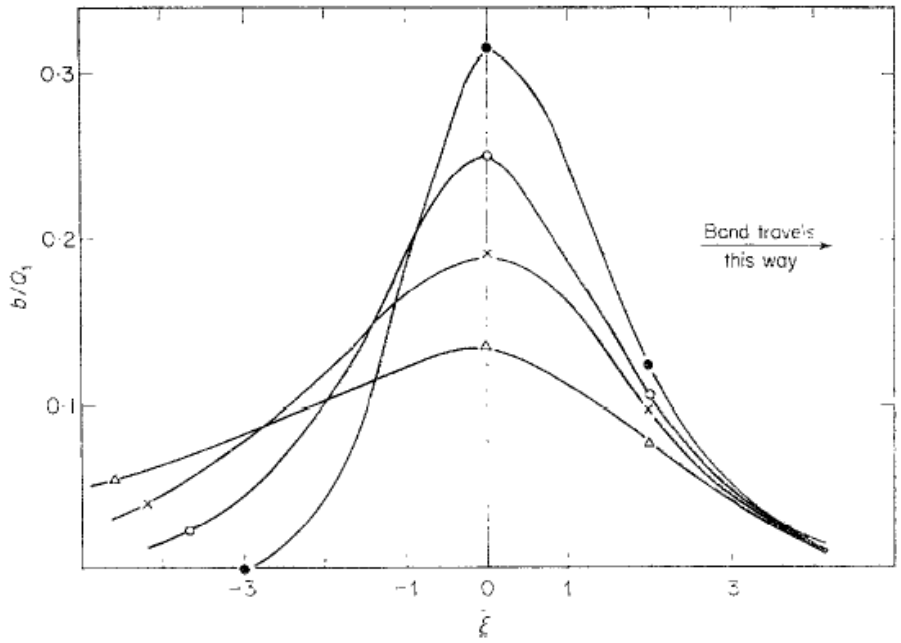

Figure 32: Bacteria band shapes investigated by Keller and Segel (1971b): ξ denotes the coordinates of the tube, $\frac{b}{Q_1}$ the bacterial density divided by a reference density

find singularities, either introduced by a step function as diffusivity function (Abraham) or by using a singular chemotactic coefficient (Keller and Segel). This is in accordance with the results obtained in this thesis, where a bounded diffusivity function and the continuous harvesting function $\frac{\alpha M}{M+k_M}$ did not allow traveling wave solutions (cf. chapter (7)). However, sufficient numerical approximations of a singular situation by means of continuous functions yielded wavelike phenomena with similar shapes (cf. section (9.2)). Section (9.3) showed that it is also possible to obtain somehow traveling waves by choosing suitable initial conditions (linear mussel spread, homogenous starfish density), though they do not correspond to the biological situation, where starfish invade an untouched mussel bed.

10 Advection-diffusion model with non-homogenous mussel distribution

The previous chapter showed that different initial conditions might be decisive if traveling waves will occur (cf. section (9.3). Thus, in this final chapter will be studied if the realistic biological scenario of a non-homogenous mussel distribution as initial condition has a strong influence on the starfish wavefront progression. The simulations in chapter (5) were all carried out with a uniform mussel distribution as initial condition. This corresponds to a situation, where the mussel beds are spread over a huge region in a homogenous way. However, as the previous chapter showed, a change in initial conditions (linear mussel density, homogenous starfish density) had a huge impact on the resulting wavefronts. Although these initial conditions are not biologically relevant, it is of great interest if a non-homogenous mussel distribution yields the same results as the basic simulations in chapter (5). Thus, in yet another run, a different scenario was chosen. This time, the mussels are spread in periodic heaps on the sea ground. This corresponds to a situation where the mussels accumulate at certain areas on the sea bed, while there are also large regions without mussels, which is definitely realistic for specific parts of the seabed. The underlying question was, if such a scenario brings the starfish front to a halt or even prevents it from forming. Once again, the simulation was computed on an interval $x \in [0, 50]$ on a timeframe of $t \in [0, 10000]$ and with an initial starfish distribution of $S_0(x) = \frac{1}{\int_0^L \exp\left(\frac{-x^2}{5^2}\right) dx} \exp\left(\frac{-x^2}{5^2}\right)$. The diffusivity function $D(M)$ was the same as before: $D_{20}(M) = 1 - \frac{1}{1+\exp(-20M)}$.
However, this time the initial mussel distribution was set to $M_0(x) = \max(\sin(b\pi x), 0)$ (cf. figure (33)) for different parameters $b > 0$. The maximum is necessary to keep the mussel density positive at all points x in space.
The simulation was done for different values of $b \in \{0.1, 0.3, 0.6, 0.9\}$. Since the heaps are sinus shaped, it is necessary to keep the parameter b low to avoid resolution problems with the grid (250 cells on a length of 50), when the discretization is carried out (cf. figure (35)). For the named values of b, discretization yields $b\frac{\text{length of intervall}}{\text{number of grid cells}} = b\frac{50}{250} \in \{0.02, 0.06, 0.12, 0.18\} << 1$.
Figures (35), (36), (37) and (38) give the results. The lower heatmap shows a striped pattern, which visualizes the periodic mussel heaps on the sea bed. While the starfish wavefront in the upper part of figures (35) and (36) is still moving stepwise like a jump function, the transition to the smooth wavelike behaviour can already be seen in figures (37) and (38).

Total mussel abundance $M_{tot}(0) = \int_0^{50} \max(0, \sin(b\pi x))\, dx$ at time $t = 0$ for the periodic mussel density:

b	$M_{tot}(0)$
0.1	19.10
0.3	16.98
0.6	15.92
0.9	16.27

Note, in the original simulation the total mussel abundance $M_{tot}(0) = 50$.
A comparison to the uniform mussel bed yields the following conclusions:

1. Starfish maximum: Now a maximum starfish density of up to 1.5 is reached. This is because for a short time the starfish accumulate at a mussel heap and it takes them longer to move on.

2. Remarkably, the time to graze down the mussel bed is always the same (about 9700 time steps), in all the periodic simulations and does not differ too much from the original simulation (about 8700 time steps), although the total mussel abundance is different in all those cases. This means, the grazing time does not strongly depend on the initial mussel density.

3. Closely related to the question of the grazing time is the question of the wavefront propagation speed. As can be seen in figures (35), (36), (37) and (38) the starfish wave is traveling at the same speed. Thus, neither size nor position of the non-homogenous mussel distribution affect the starfish propagation speed. This means the starfish move ahead with a resulting speed which seems to be largely independent from the mussel distribution's wave length.

4. Figure (35) shows that on each of the periodic occurring mussel beds the grazing takes place in the characteristic $t^{\frac{1}{2}}$ shaped curve, which was already noticed in the original simulation.

With periodic mussel beds on the sea bed, it is more difficult to characterize and compare the resulting wavefronts, because the total mussel abundance varies with the parameter b and needs to be taken into consideration. Thus, a further analysis will be skipped here.

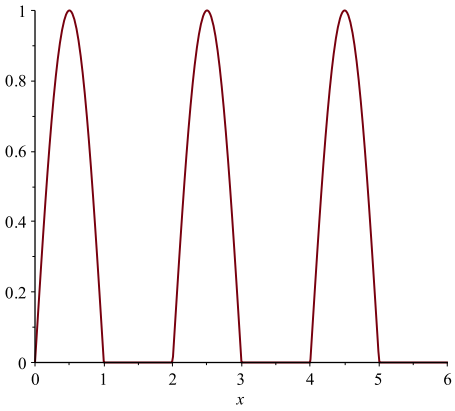

Figure 33: $\max(0, \sin(b\pi x))$ on $[0, 6]$ for $b = 1$

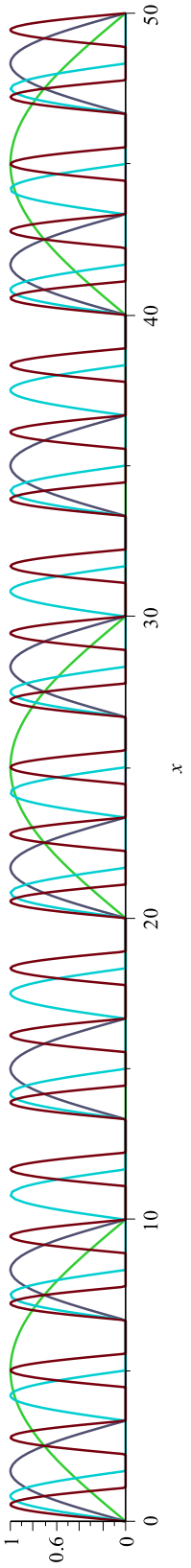

Figure 34: Periodic initial condition with mussel density: $M(x, 0) = \max(0, \sin(b\pi x))$ for $b = 0.1$ (green), $b = 0.3$ (dark blue), $b = 0.6$ (light blue), $b = 0.9$ (magenta)

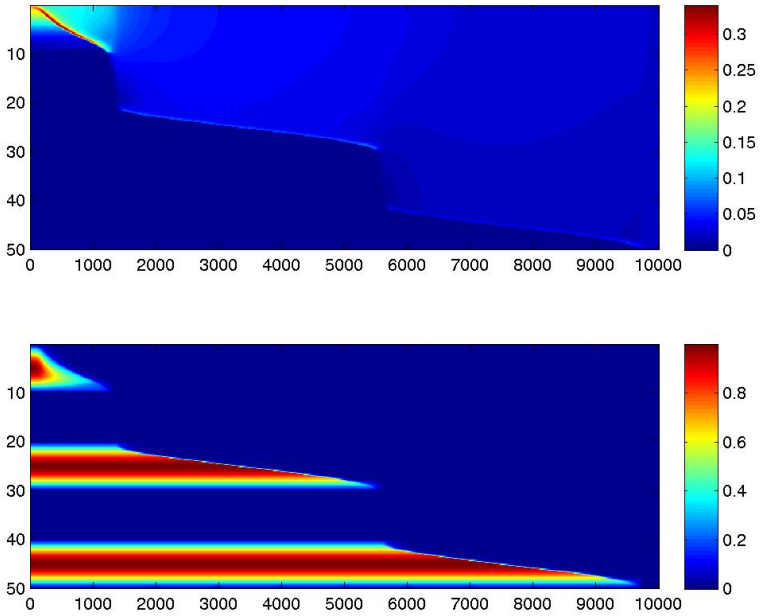

Figure 35: Heatmap for periodic initial mussel bed: $M(x,0) = \max(0, \sin(b\pi x))$ with b=0.1

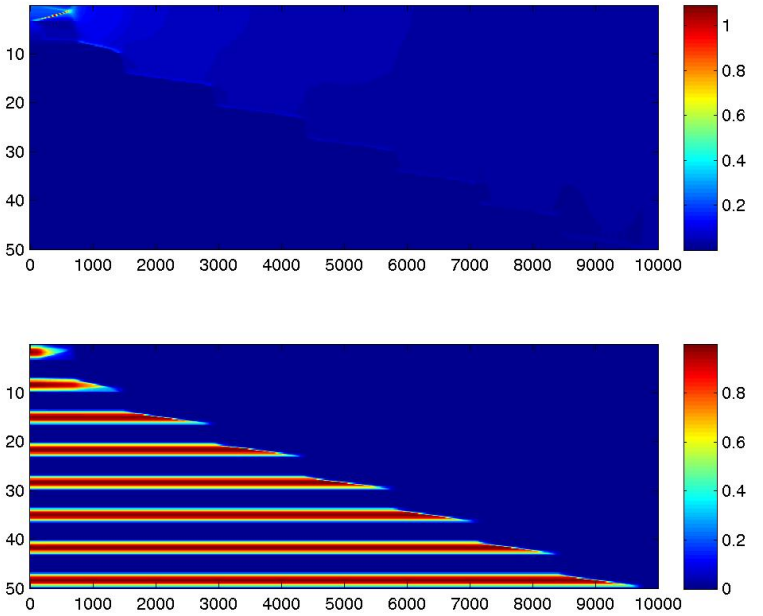

Figure 36: Heatmap for periodic initial mussel bed: $M(x,0) = \max(0, \sin(b\pi x))$ with b=0.3

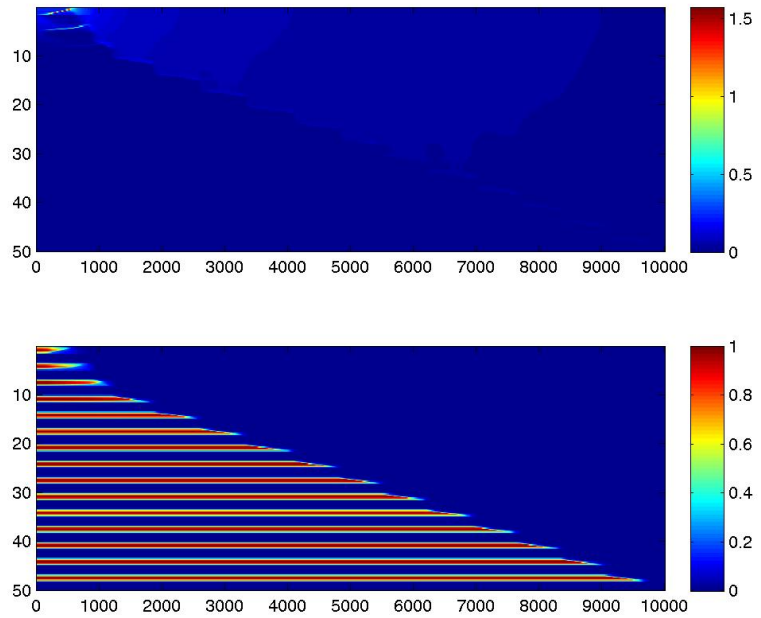

Figure 37: Heatmap for periodic initial mussel bed: $M(x,0) = \max(0, \sin(b\pi x))$ with b=0.6

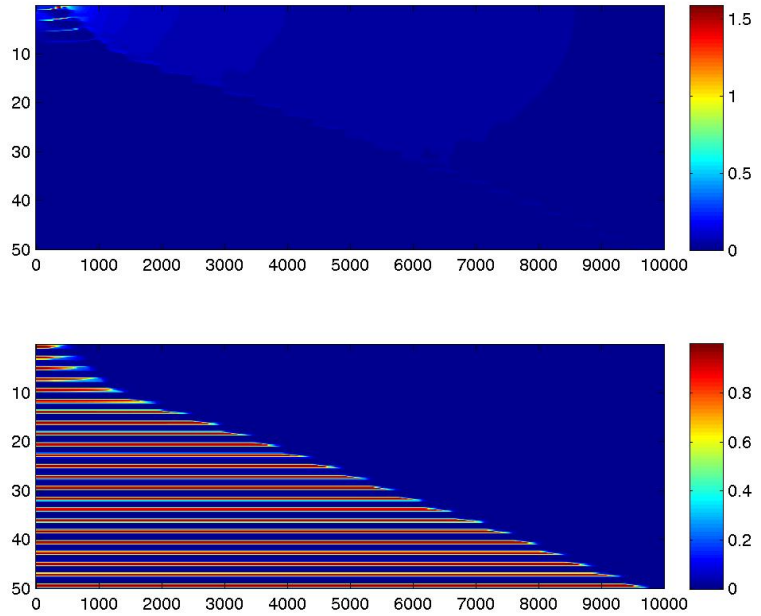

Figure 38: Heatmap for periodic initial mussel bed: $M(x,0) = \max(0, \sin(b\pi x))$ with b=0.9

11 Conclusion

The aim of this thesis was to model starfish $S(x,t)$ feeding on mussels $M(x,t)$ in the Danish Limfjord by means of the following advection-diffusion model with reasonably chosen harvesting $h(M(x,t))$ and diffusivity function $D(M(x,t))$:

$$\boxed{\begin{aligned}\frac{\partial S(x,t)}{\partial t} &= \frac{\partial^2}{\partial x^2}\left[D(M(x,t))S(x,t)\right] \\ \frac{\partial M(x,t)}{\partial t} &= -\,h(M(x,t))S(x,t)\end{aligned}}$$

The numerical simulations of this model actually produced a clearly recognisable starfish wave invading the mussel bed and thus corresponded to the biological observations. In contrast to traveling waves in a classical sense these starfish wavefronts have decreasing amplitude and a certain amount of starfish stays behind in a tail. It turned out that the amplitude of the wavefront followed a power law of $\approx t^{-1}$. However, starfish entropy and the mussel wavefront position followed rather a power law of $\approx t^{\frac{1}{2}}$. The hypothesis that the system might be scaling-invariant seemed promising, though further investigations will be necessary to find the most suitable scaling function. In an analytical approach it could be shown that the PDE system does not allow traveling invasion waves as solutions. This corresponds to the waves obtained in the simulations, which were similar to but not actual traveling waves. Additionally, it was investigated how much the system's stability is affected by the diffusivity function if one includes mussel growth into the PDE. The result of the linear stability analysis was that in case of a stable non-spatial system, a corresponding spatial system will always be stable as well. On the contrary, it is possible to stabilize an unstable non-spatial system by choosing an appropriate diffusivity function.

All those results were compared to other scientists' findings. It was explained under which biological assumptions they managed to obtain traveling wave solutions and stated that their assumptions are not always reasonable from a biological point of view. By adapting the parameters to create similar scenarios as in their models, it was possible to obtain wavelike phenomena approximating actual traveling waves. Of special interest were the findings by Keller and Segel (1971b), who proved that differing wavefront shapes can be explained by the parameters used in the diffusivity and harvesting function. This gives evidence that the different shapes obtained in Abraham (2007) and the model presented in this thesis are due to different parameter choices. Finally, simulations with periodic mussel beds as initial conditions showed that this scenario does not keep the

starfish from forming a wavefront. This means that the actual distribution of the mussels on the seabed will in general not strongly affect the starfish wavefront progression.
Since the advection-diffusion model introduced in this thesis is generally based on biologically reasonable conditions, it gives valuable evidence that diffusivity and harvesting processes are able to evoke wavelike behaviour in predators such as starfish. The model parameters and initial conditions can be adapted to data obtained through field work. This makes it possible to better understand starfish wavefronts feeding on mussel beds and to improve the prediction of starfish invasions and their impact on the mussel population, which is an important issue for biologists and fishers working at the Limfjord.

12 Outlook

This section is the collection of some ideas, how to further improve the model and adapt the model to the given biological scenario so that starfish invasions can be even better understood and predicted.

The numerical simulations in this master thesis were carried out for a one-dimensional seabed strip. From a biological point of view, it would be highly interesting to redo the simulations on a two-dimensional grid. While the results on a rectangular area might be similar to the wavelike phenomena occurring in the one-dimensional case, an oddly shaped seabed strip containing obstacles (rocks, trenches, aso.) could significantly disturb the waves in their progression. Thus, measures to bring the invasion wave to a halt can be investigated.

Sea arms and confined areas such as the Limfjord raise the question, what will happen after the starfish invasion. For biologists, fishers and environmentalists it is important to know, how soon a second wave might invade the area. Starfish proliferation as well as starving in absence of prey could be added to the model to investigate this scenario.

Another interesting issue would be the introduction of a threshold M_0 into the diffusivity function, e.g. $D(M) = \frac{1}{1+\exp(k(M-M_0))}$. This corresponds to a situation where the starfish do not change their progression in presence of small amounts of mussels, but start slowing down rather quickly when the mussel density lies above a specific threshold. Additionally, further simulations with different harvesting functions might be of interest, since the speed of the mussel consumption has a strong effect on the starfish wavefront progression.

Up to now, starfish interaction was not taken into consideration, since this issue has not been profoundly investigated by biologists yet. It is not known, if starfish tend to keep close to or far from their kind, while searching prey. However, any form of interaction between the starfish would definitely have a huge impact on the system's dynamics.

At the time this master thesis was handed in, the data from recent mussel and starfish counts in the Limfjord were not yet available. Since initial conditions had a strong influence on the resulting wave (cf. traveling wave in figure (29) vs. resulting wave in figure (12)), it is suggested to redo the simulations with adapted initial conditions, as soon as biological data is available.

13 Abstract in English

The Danish Limfjord is famous for its mussel beds, which are harvested by fishers and known to be a popular delicacy. However, it has been observed that starfish waves invade former untouched mussel beds and completely erase them during their progression. The aim of this master thesis was to develop a PDE model describing this phenomenon.
During the numerical simulations (MOL), it turned out that an advective-diffusive approach with suitable functions to specify starfish diffusion and mussel harvesting, actually yields wavelike solutions. However, these waves are not traveling waves in the classical sense, since amplitude and speed change over time. Thus, the obtained data was used to analyze and study their characteristics and asymptotics. Of special interest is the observation that some starfish are not part of the wavefront, but rather stay behind. Entropy is used as a measure to describe this phenomenon with a powerlaw ansatz.
In accordance with these results is the analytical proof that for the given PDE model traveling invasion waves cannot occur. A natural model extension would be to include mussel growth. At first glance, it is not clear if this could affect the system's stability. The calculations carried out in this thesis showed that a stable non-spatial system will remain stable, no matter which diffusivity function will be used to describe the spatial system. Further, it is actually possible to stabilize an unstable non-spatial system by adequately choosing the diffusivity function.
A comparison to other scientists' results yielded that they were actually able to get traveling wave solutions in similar models by introducing singularities. Hence, in another simulation run the parameters were chosen to approximate their initial conditions and diffusivity functions. Indeed, this resulted in traveling waves. Although it has to be stated that the biological assumptions do not correspond to a realistic scenario.
Finally, it was investigated how periodic mussel beds as initial condition affect the wavelike starfish invasion. It turned out that the results are quite similar to the case with homogenous mussel distribution. This means that the actual mussel bed shapes, be it heap-like or rather uniformly spread, are not of high significance.
Summing up all those findings, one can conclude that the advection-diffusion PDE model is able to model starfish invasions in a quite satisfying manner. From a mathematical point of view, it is highly interesting to compare the starfish waves to traveling waves as known from PDE theory and develop ways to characterize them. From a biological point of view, it is of high value to learn about the starfish wavefront's characteristics as to have a better understanding how fast and intense the mussel harvesting progresses.

14 Abstract in German

Der Limfjord in Dänemark ist berühmt für seine Miesmuschelbänke, die von Fischern geerntet werden und eine beliebte Delikatesse darstellen. Immer wieder treten jedoch wellenartige Seesterninvasionen auf, die in die Muschelbänke einfallen und diese im Zuge ihrer Wanderung völlig abernten. Ziel dieser Diplomarbeit war die Entwicklung eines PDE-Modells zur Beschreibung und Analyse dieses Phänomens.

In den numerischen Simulationen (Linienmethode) zeigte sich, dass ein Advektions-Diffusions-Ansatz mit geeigneter Diffusivitätsfunktion für die Fortbewegung der Seesterne und Erntefunktion für die Muschelbänke tatsächlich wellenartige Lösungen hervorbringt. Im Gegensatz zu den traveling waves aus der klassischen PDE-Theorie ändern diese Wellen jedoch im Laufe der Zeit Amplitude und Form. Die Daten aus den Simulationen wurden für eine gründliche Analyse der Wellengestalt verwendet, wobei sich herausstellte, dass einige Seesterne stets hinter der Wellenfront zurückblieben. Um dieses Phänomen mit einem powerlaw-Ansatz zu beschreiben, wurde Entropie als Maß verwendet.

In Übereinstimmung mit den bisher erwähnten Resultaten ist der analytische Beweis, dass für das Modell in dieser Diplomarbeit keine echten traveling-wave-Lösungen existieren. Es ist daher naheliegend ein erweitertes Modell, das auch Muschelwachstum berücksichtigt, zu untersuchen. In einer linearen Stabilitätsanalyse zeigte sich, dass die Stabilität beim Übergang von einem Modell ohne zu einem mit Diffusion stets erhalten bleibt. Umgekehrt kann eine geeignet gewählte Diffusivitätsfunktion sogar ein instabiles System stabilisieren.

Anschließend wurden die Ergebnisse noch mit den Erkenntnissen anderer Forscher verglichen, die in ähnlichen Modellen traveling-wave-Lösungen vorweisen konnten. Es stellte sich heraus, dass dies durch die Verwendung von Singularitäten (z.B. unstetige Diffusivitätsfunktion) möglich war und es sei angemerkt, dass die in diesen Modellen getroffenen Annahmen nicht unbedingt den biologischen Gegebenheiten entsprechen. Wurden die Parameter des Advektions-Diffusions-Modells an diese Szenarien angepasst, so zeigten sich ebenfalls traveling-wave-artige Lösungen in den Simulationen.

Zum Abschluss wurde noch untersucht, wie sich eine nicht-homogene Anfangsbedingung, d.h. periodische Muschelanhäufungen am Meeresgrund, auf die Seesterninvasionswellen auswirkt. Es zeigte sich, dass die Simulation im Wesentlichen die gleichen Ergebnisse wie im homogenen Fall lieferte und daher die konkrete Form der Muschelbänke im Allgemeinen keinen großen Einfluss auf die Seesterninvasion hat.

Zusammenfassend kann festgehalten werden, dass das entwickelte Modell die biologische Dynamik und die realen Gegebenheiten äußerst zufriedenstellend beschreibt. Vom

mathematischen Standpunkt sind dabei besonders die auftretenden Wellen interessant und eine Gegenüberstellung bzw. mögliche Einordnung in die Theorie der traveling-wave-Lösungen. Vom biologischen Standpunkt ist es erfreulich, dass mit diesem Modell Seesterninvasionen besser untersucht werden können und sich dadurch entscheidende Rückschlüsse auf das Abernten der Muschelbänke ziehen lassen.

15 List of Figures

16 References

Abraham, E. R. 2007. Sea-urchin feeding fronts. *Ecological Complexity* 4:161–168.

Begon, M., Townsend, C. R., and Harper, J. L. 2006. Ecology: From Individuals to Ecosystems. Blackwell Publishing, 4^{th} edition.

Campos, J., Guerrero, P., Sánchez, O., and Soler, J. 2013. On the analysis of traveling waves to a nonlinear flux limited reaction-diffusion equation. *Ann. I. H. Poincaré* 30:141–155.

Dare, P. J. 1982. Notes on the swarming behaviour and population density of asterias rubens l. (echinodermata: Asteroidea) feeding on the mussel, mytilus edulis l. *J. Cons. Int. Mer.* 40:112–118.

Gardiner, C. W. 2002. Handbook of Stochastic Methods. Springer-Verlag, 2^{nd} edition.

Hamid, S., Schiesser, W. E., and Griffiths, G. W. 2007. Method of lines.

Holling, C. 1959. Some characteristics of simple types of predation and parasitism. *The Canadian Entomologist* XCI:385–398.

Keller, E. F. and Segel, L. A. 1971a. Model for chemotaxis. *Journal of Theoretical Biology* 30:225–234.

Keller, E. F. and Segel, L. A. 1971b. Traveling bands of chemotactic bacteria: A theoretical analysis. *Journal of Theoretical Biology* 30:235–248.

Lauzon-Guay, J.-S., Scheling, R. E., and Barbeau, M. A. 2008. Formation and propagation of feeding fronts in benthic marine invertebrates: A modeling approach. *Ecology* 89:3150–3162.

Murray, J. 2001. Mathematical Biology I: An Introduction, volume 17 of *Interdisciplinary Applied Mathematics*. Springer-Verlag, 3. edition.

Murray, J. 2003. Mathematical Biology II: Spatial Models and Biomedical Applications, volume 18 of *Interdisciplinary Applied Mathematics*. Springer-Verlag, 3. edition.

Norberg, J. and Tedengren, M. 1995. Attack behaviour and predatory success of asterias rubens l. related to differences in size and morphology of the prey mussel mytilus edulis l. *Journal of Experimental Marine Biology and Ecology* 186:207–220.

Saier, B. 2001. Direct and indirect effects of seastar asterias rubens on mussel beds (mytilus edulis) in the wadden sea. *Journal of Sea Research* 46:29–42.

Scheibling, R. E. and Lauzon-Guay, J.-S. 2007. Feeding aggregations of sea stars (asterias spp. and henricia sanguinolenta) associated with sea urchin (strongylocentrotus droebachiensis) grazing fronts in nova scotia. *Marine Biology* 151:1175–1183.

Schiesser, W. E. 1991. The Numerical Method of Lines: Integration of Partial Differential Equations. Acad. Press.

Shigesada, N. and Kawasaki, K. 1997. Biological Invasions: Theory and Practice. Oxford University Press.